Mechanistic Modelling of Drug-Induced Liver Injury: Investigating the Role of Innate Immune Responses

Lisl KM Shoda[1], Christina Battista[1,2], Scott Q Siler[1], David S Pisetsky[3], Paul B Watkins[2] and Brett A Howell[1]

[1]DILIsym Services, Inc., Research Triangle Park, NC, USA. [2]UNC Institute for Drug Safety Sciences, University of North Carolina at Chapel Hill, Research Triangle Park, NC, USA. [3]Medical Research Service, Durham VA Medical Center and Duke University Medical Center, Durham, NC, USA.

Gene Regulation and Systems Biology
Volume 11: 1–22

DOI: 10.1177/1177625017696074

ABSTRACT: Drug-induced liver injury (DILI) remains an adverse event of significant concern for drug development and marketed drugs, and the field would benefit from better tools to identify liver liabilities early in development and/or to mitigate potential DILI risk in otherwise promising drugs. DILIsym software takes a quantitative systems toxicology approach to represent DILI in pre-clinical species and in humans for the mechanistic investigation of liver toxicity. In addition to multiple intrinsic mechanisms of hepatocyte toxicity (ie, oxidative stress, bile acid accumulation, mitochondrial dysfunction), DILIsym includes the interaction between hepatocytes and cells of the innate immune response in the amplification of liver injury and in liver regeneration. The representation of innate immune responses, detailed here, consolidates much of the available data on the innate immune response in DILI within a single framework and affords the opportunity to systematically investigate the contribution of the innate response to DILI.

KEYWORDS: Quantitative systems pharmacology (QSP), quantitative systems toxicology (QST), mechanistic modelling, DILIsym, DILI, immune

RECEIVED: September 30, 2016. **ACCEPTED:** February 4, 2017.

PEER REVIEW: Six peer reviewers contributed to the peer review report. Reviewers' reports totalled 1210 words, excluding any confidential comments to the academic editor.

TYPE: Original Research

FUNDING: The author(s) disclosed receipt of the following financial support for the research, authorship, and/or publication of this article: This project was supported in part by an appointment (C.B.) to the Research Participation Program at the Center for Drug Evaluation and Research, U.S. Food and Drug Administration, administered by the Oak Ridge Institute for Science and Education through an interagency agreement between the U.S. Department of Energy and FDA.

DECLARATION OF CONFLICTING INTERESTS: The author(s) declared no potential conflicts of interest with respect to the research, authorship, and/or publication of this article.

CORRESPONDING AUTHOR: Lisl KM Shoda, DILIsym Services Inc., Six Davis Drive, Research Triangle Park, NC 27709, USA. Email: lshoda@dilisym.com

Introduction

DILI is an important safety concern in drug development and approved use that can lead to termination of development programs, changes to the drug label, and market withdrawal[1–4]. The multiplicity of contributors to DILI and the persistent need for better predictive models has fuelled the establishment of a public-private partnership, The DILI-sim Initiative currently consists of scientists from academia, the FDA, and 12 major pharmaceutical companies. The DILI-sim Initiative has sponsored the development of successive versions of DILIsym software (currently v5A), detailing a mechanistic model of DILI in pre-clinical species and in humans. In this paper, we describe DILIsym with particular attention to the innate immune response following drug exposure and its contribution to injury progression and resolution.

Although the etiology of DILI events is rarely known, several putative mechanisms of toxicity have been implicated through *in vitro* studies. For example, extensive study of acetaminophen (APAP) induced liver injury has demonstrated that hepatocytes metabolize APAP to a reactive metabolite, whose actions produce oxidative stress, ultimately leading to hepatocyte necrosis[5]. Other studies have demonstrated that compounds that inhibit the bile salt export pump (BSEP), a hepatic bile acid efflux transporter, alone or with concurrent inhibition of multidrug resistance-associated proteins (MRPs), are disproportionately represented amongst compounds with DILI liability[6,7]. Still another study has demonstrated that compounds with dual activity inhibiting BSEP and inducing mitochondrial dysfunction are associated with more severe human DILI[8]. These and similar studies provide information on mechanisms of hepatotoxicity that may be directly attributed to the compound or its metabolites.

In addition to direct effects of compounds on hepatocytes, it is likely that the occurrence of DILI is also determined by patient-specific attributes, which could include normal inter-individual variability, disease state(s), nutritional and immune status[9]. Immune responses may be mediated by innate immune cells (*e.g.*, macrophages, neutrophils, NK cells, dendritic cells) and/or by adaptive immune cells (*e.g.*, T and B cells). The former can respond rapidly to stimulation by infection or injury and are considered the first-line defense against an infectious insult. The latter initially respond more slowly, as the small number of T and B cells that can specifically recognize the infectious agent, proliferate and differentiate to develop the cell numbers and specialized activities to address the immune challenge. Importantly, innate immune cells are required participants in the development of an adaptive immune response[10,11]. Innate immune responses have been characterized for a few drugs that can predictably induce DILI in experimental animal models (*e.g.*, APAP)[12,13]. In contrast, adaptive immune responses have been implicated for some compounds that induce DILI only rarely, with delayed onset, and often with evidence of a more rapid response on re-challenge[14]. Early identification of compounds associated with rare DILI arguably represents the greatest unmet need for drug development.

DILIsym applies quantitative systems pharmacology (QSP) to this toxicology challenge, *i.e.*, quantitative systems toxicology (QST). DILIsym is an ongoing developmental effort generating a mechanistic representation of DILI in pre-clinical species and in humans for prospective predictions and retrospective analyses. The mechanistic representation includes essential cellular processes in multiple interacting sub-models, *e.g.*, physiologically based pharmacokinetics (PBPK), oxidative stress, bile acid-mediated toxicity, mitochondrial dysfunction, lipotoxicity, hepatocyte life cycle, and macrophage and endothelial cell life cycles. Interaction amongst sub-models integrates compound exposure with direct mechanisms of compound toxicity and elicited immune responses which may mathematically combine to produce liver injury. Equations describing biochemical relationships and parameter values for those relationships have largely been constructed based on data from the published literature. Parameter values characterizing responses to compounds have been optimized through the inclusion of exemplar compounds within DILIsym (*e.g.*, APAP, glibenclamide), illustrating the application of compounds in model development. The utility of this approach has been and continues to be assessed in the analysis of compounds that were not used in optimization (*e.g.*, AMAP, tolcapone, troglitazone, as well as many other proprietary compounds currently in development), generating predictions of hepatotoxicity risk. The reader is referred to other publications for general descriptions of DILIsym as well as for simulation-based predictions of hepatotoxicity by compounds not used in model development[15–18].

What follows is a review of model development for an innate immune response in DILIsym, including key literature, equations, parameter values, and comparisons between simulation results and experimental data. The inclusion of the innate response permits the investigation of its contribution to hepatotoxicity or recovery, as well as the analysis of how inter-individual variability in immune responsiveness may affect the manifestation of liver injury.

Model Development

General Modelling Approach

DILIsym consists of multiple interacting sub-models (Figure 1). Additions to DILIsym are executed in multiple stages: scoping, sub-model development, integration, and qualification. During the scoping phase, the literature is assessed to identify key components for inclusion in the sub-model and to assess the availability of data to support parameter selection and the availability of comparator data for simulated behaviours. The approach is to model only to the level of detail required to reproduce the majority of comparator data. In sub-model development, the equations are developed and baseline parameter values are selected. The integration phase is an iterative process that includes using DILIsym values as inputs to the sub-model and allowing the new sub-model to dynamically influence existing sub-models within DILIsym

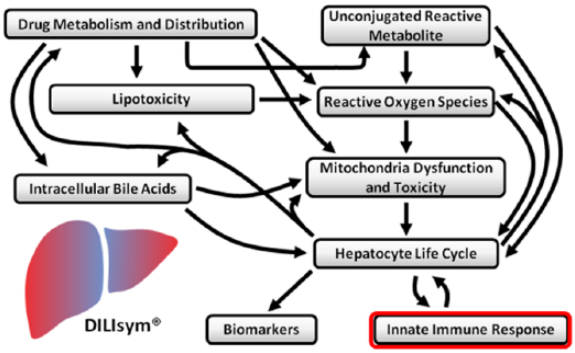

Figure 1. Schematic overview of the sub-models and their interactions in DILIsym.

(*e.g.*, hepatocyte life cycle). In this phase, simulations of exemplar compounds may be used to further inform parameter selection such that simulated results are consistent with the majority of the comparator data. Finally, in the qualification phase, the behaviour of the new sub-model is characterized with different compounds and under different experimental conditions. In this phase, simulation results reflect new inputs only, not further parameter changes, and thus serve to test the new sub-model and by extension, the overall integrated model.

Scoping Phase

Scoping of immune responses in DILI quickly revealed that, while there appears to be broad support for the involvement of immune responses, there are fewer data available than one might expect. APAP is the dominant compound for which immune data have been collected, although some data are available for others, *e.g.*, halothane, amodiaquine, isoniazid[19–21]. Further, the vast majority of immune-related data are derived from mouse models. DILIsym development has taken a step-by-step approach in starting with an innate immune response, with an initial focus on the response to APAP in mouse models.

APAP is the most extensively studied compound with liver liabilities. Overdose reproducibly induces liver injury in mouse models and in humans. APAP metabolism and the initial intra-hepatocyte events that contribute to early intrinsic toxicity are well characterized[5]. Briefly, APAP can be metabolized by CYP3A4 and CYP2E1 enzymes to yield a reactive metabolite, *N*-acetyl-*p*-benzoquinone imine (NAPQI). NAPQI can be neutralized by glutathione (GSH) conjugation. However, excess NAPQI, as seen in overdose, depletes GSH, leading to excess reactive oxygen and nitrogen species and oxidative stress. High levels of oxidative stress induced by APAP overdose induce hepatocyte necrosis, initiating liver damage[5,22].

An immune response has been shown to follow APAP metabolism and NAPQI-mediated cell death. Hepatocyte necrosis releases intracellular molecules that can activate immune cells, known as damage-associated molecular pattern

(DAMP) molecules or DAMPs. DAMPs have also been termed danger molecules to reflect their role as indicators of cell injury and death, mobilizing immune cells to action[23]. DAMPs can interact with the same receptors as pathogen associated molecular patterns (PAMPs) such the toll-like receptors (TLR), with receptor activation inducing inflammation in the absence of infection, *i.e.*, sterile inflammation.

High mobility group box 1 (HMGB1) protein is one such DAMP. HMGB1 is a non-histone nuclear protein that binds DNA and has activity in transcription and regulation of chromosome structure. The activity of HMGB1 depends on post-translational modification as well as redox events affecting three sulfydryl groups at positions 23, 45 and 106[24]. Finally, HMGB1 can be acetylated during the activation of immune cells. Total circulating HMGB1, as well as the acetylated form, have been shown to increase in APAP DILI in both mice and in humans[25,26]. Interestingly, pharmacologic blockade of HMGB1 or genetic silencing of HMGB1 in hepatocytes has been shown to reduce the severity of APAP DILI in mice[27–30], emphasizing its apparent contribution to injury. HMGB1 has been shown to activate macrophages[31–33], and macrophages are plentiful in the liver, where a resident population, termed Kupffer cells, accounts for 80% of the whole body tissue macrophage population[34].

Under normal conditions, liver macrophages likely contribute to the liver's overall function of detoxification and clearance by phagocytosing and eliminating dying cells or cellular fragments and by presenting gut-derived antigens to T cells to promote immune tolerance (and prevent errant immune response)[34–36]. Under inflammatory conditions, such as those associated with hepatocyte necrosis, liver macrophages are not only activated by DAMPs but also accumulate[37]. DAMP-activated liver macrophages likely participate in the clearance of dying hepatocytes but also produce cytokines, such as tumour necrosis factor alpha (TNF-α) that can mediate further injury but may also be involved in regeneration[38,39].

Besides macrophages, there are other innate immune cells that are resident to the liver (*e.g.*, NK cells) or accumulate under inflammatory conditions (*e.g.*, neutrophils) and may contribute to APAP DILI. However, it has been difficult to definitively show the contribution of many of these cell types, in part due to redundancy within the immune response, where most functions (*e.g.*, phagocytosis, TNF-α production, contact-mediated cytotoxicity) can be carried out by multiple cell types. This redundancy makes it difficult to quantify the effects attributed to the absence of a particular cell type when compensatory pathways are likely engaged. Additionally, many of the experimental techniques used to deplete or inhibit a cell type have ancillary effects that complicate the interpretation of results. For example, pharmacologic depletion or inhibition of NK cells, NKT cells, and neutrophils has been used to illustrate their role in APAP DILI[40–42]. However, other studies have shown that the pharmacologic manipulation independently modified APAP distribution or metabolism, thus affecting not only the immune cell of interest but also the APAP-induced intrinsic injury, and complicating the interpretation[43].

The effects of macrophage depletion have been investigated through the administration of liposome-encapsulated clodronate[44–48]. This methodology does not appear to suffer some of the drawbacks of other pharmacologic interventions discussed above, and early results indicate that macrophage depletion exacerbates APAP DILI, which was interpreted as demonstrating a net protective or regenerative role of liver macrophages[44]. However, even in this case where the methodology is not in question, further investigation has modified the interpretation. Namely, the observed effect of clodronate on injury has ranged from exacerbation to no effect[45–48], and the interpretation has evolved from a role of macrophages as mediating an early anti-inflammatory or pro-regenerative effect to macrophages as acting later to speed recovery and regeneration[47].

Finally, there are structural cells in the liver, particularly the liver sinusoidal endothelial cells (LSECs), which are not immune cells per se, but may contribute to immune-mediated injury or regeneration. LSECs line the liver sinusoids, delineating the physical boundary between hepatocytes and circulating blood. Contrary to endothelial cells elsewhere in the body, LSECs form only a loose and highly permeable barrier, with distinctive fenestrations measuring roughly 100 nm that permit free passage of soluble molecules or cellular protrusions, *e.g.*, hepatocyte microvilli[34]. Nevertheless, LSECs likely regulate the accumulation of immune cells via mediator production and adhesion molecule expression[34]. *In vitro* assays suggest that APAP can mediate LSEC cytotoxicity, and *in vivo* studies in mice provide microscopic and biochemical evidence for altered morphology and function following APAP overdose[49–51].

As discussed above, the initial immune scoping effort considered the available data across species, compounds, immune cell types, and mediators. Based on a review of the literature, the initial immune sub-model focused primarily on the representation of liver macrophages in the APAP response, including activation by DAMPs, accumulation, production of mediators, and effects on injury and regeneration. A minimal representation of LSECs was also developed. The overall approach includes maintaining as simple a representation as possible, while allowing for the possibility of future expansion and/or refinement.

Sub-Model Development

Liver Macrophage Life Cycle. The liver macrophage life cycle was loosely based on the pre-existing DILIsym hepatocyte life cycle. The structure allows for recruitment of precursor cells (*i.e.*, monocytes) from circulation, maturation from an immature liver macrophage state to a mature liver macrophage state, *in situ* proliferation, and apoptosis (Figure 2). The population size and characteristics are determined by the following set of differential equations:

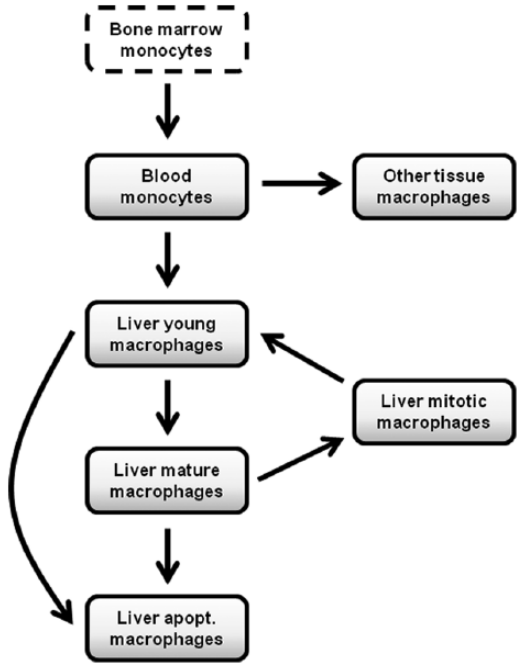

Figure 2. Schematic of liver macrophage life cycle as represented in DILIsym. Solid lined boxes delineate the various sub-populations and movement amongst them. Blood monocytes are derived from a source, conceptually bone marrow monocytes, but the latter are not quantitatively tracked as indicated by the dashed line.

Blood monocytes

$$\frac{dMo}{dt} = \alpha BV - \beta Mo - Mo \sum_{j=\{pp,ml,cl\}} RR_{mac,j} \quad (1)$$

Immature liver macrophages

$$\frac{dI_{mac,j}}{dt} = 2\gamma_{mac} C_{mac,j} + Mo\, RR_{mac,j} - I_{mac,j}\, MR_{mac,j} - IDR_{mac,j} \quad (2)$$

Mature liver macrophages

$$\frac{dM_{mac,j}}{dt} = I_{mac,j}\, MR_{mac,j} - M_{mac,j}\, PR_{mac,j} - M_{mac,j}\, AR_{mac,j} - MDR_{mac,j} \quad (3)$$

Mitotic liver macrophages

$$\frac{dC_{mac,j}}{dt} = M_{mac,j}\, PR_{mac,j} - \gamma_{mac} C_{mac,j} \quad (4)$$

Apoptotic liver macrophages

$$\frac{dA_{mac,j}}{dt} = M_{mac,j}\, AR_{mac,j} - A_{mac,j} \frac{\log 2}{CL_{apop}} MDR_{mac,j}, \quad (5)$$

where Mo represents the blood monocytes and $I_{mac,j}$, $M_{mac,j}$, $C_{mac,j}$, and $A_{mac,j}$ represent the immature, mature, mitotic, and apoptotic liver macrophage populations, respectively, in liver zone j, where j is either the periportal (pp), midlobular (ml), or centrilobular (cl) region. The symbol α reflects the influx of monocytes from bone marrow to circulation; β is a rate constant representing the non-liver recruitment of macrophages; γ_{mac} is the rate of mitosis for macrophages; and BV is the blood volume. $RR_{mac,j}$, $MR_{mac,j}$, $PR_{mac,j}$, and $AR_{mac,j}$ are the macrophage recruitment, maturation, proliferation, and apoptotic rates, respectively, in each zone j of the liver. $IDR_{mac,j}$ is the immature macrophage depletion rate and $MDR_{mac,j}$ is the mature macrophage depletion rate. The apoptotic clearance time constant is denoted by CL_{apop}.

Macrophage life cycle parameter values were derived from the published literature and are listed in Table 1.

LSEC Life Cycle. In this initial representation, LSECs were designed to play a relatively simple functional role in mediator production and immune cell recruitment. The associated LSEC life cycle is simpler than the macrophage life cycle, accounting only for maturation from an immature state to a mature state, *in situ* proliferation, and apoptosis. The population is determined by the following set of differential equations:

Immature liver LSECs

$$\frac{dI_{lsec,j}}{dt} = 2\gamma_{lsec} C_{lsec,j} - I_{lsec,j}\, MR_{lsec} \quad (6)$$

Mature liver LSECs

$$\frac{dM_{lsec,j}}{dt} = I_{lsec,j}\, MR_{lsec} - M_{lsec,j}\, PR_{lsec,j} - M_{lsec,j}\, AR_{lsec,j} \quad (7)$$

Mitotic liver LSECs

$$\frac{dC_{lsec,j}}{dt} = M_{lsec,j}\, PR_{lsec,j} - \gamma_{lsec} C_{lsec,j} \quad (8)$$

Apoptotic liver LSECs

$$\frac{dA_{lsec,j}}{dt} = M_{lsec,j}\, AR_{lsec,j} - A_{lsec,j} \frac{\log 2}{CL_{apop}} \quad (9)$$

where $I_{lsec,j}$, $M_{lsec,j}$, $C_{lsec,j}$, and $A_{lsec,j}$ represent the immature, mature, mitotic, and apoptotic LSEC populations, respectively, in liver zone j. Similar to the parameters defined for the liver macrophage life cycle, MR_{lsec}, $PR_{lsec,j}$, and $AR_{lsec,j}$ are the LSEC maturation, proliferation, and apoptotic rates. It should be noted that $PR_{lsec,j}$ and $AR_{lsec,j}$ are zone-dependent while MR_{lsec} remains constant throughout the liver. Lastly, γ_{lsec} is the mitosis rate for LSECs and CL_{apop} is the apoptotic clearance rate.

LSEC life cycle parameter values were derived from the published literature and are listed in Table 2.

Mediator Production, Regulation, and Effects. Initially, a minimal set of mediators has been represented, including TNF-α, HMGB1, IL-10, and hepatocyte growth factor (HGF). TNF-α is produced by activated macrophages and LSECs[52–54]. Acetylated HMGB1 (acHMGB1) is secreted by activated

Table 1. Mouse macrophage life cycle parameter values.

PARAMETER	DESCRIPTION	MOUSE VALUE	UNITS	SOURCES§
α	Influx of monocytes from bone marrow to circulation	4.5e-5	10^9 cells/hr/mL blood	99,100
β	Rate constant representing non-liver recruitment of macrophages	0.0812	1/hr	100
γ_{mac}	Rate of mitosis for macrophages	0.0416	1/hr	101–104
BV	Blood volume	1.225	mL	105
$RR_{mac,j}$ *(pp/ml/cl)**†	Macrophage recruitment rate	0.0234/0.0105/0.0023	1/hr	100,106,107
$MR_{mac,j}$ *(pp/ml/cl)**	Macrophage maturation rate	0.014/0.014/0.014	1/hr	92
$PR_{mac,j}$ *(pp/ml/cl)**	Macrophage proliferation rate	5.3e-4/5.3e-4/5.3e-4	1/hr	98,106–111
$AR_{mac,j}$ *(pp/ml/cl)**	Macrophage apoptotic rate	0.0033/0.0033/0.0033	1/hr	Calculated
$IDR_{mac,j}$ *(pp/ml/cl)** ‡	Immature macrophage depletion rate	0/0/0	10^9 cells/hr	–
$MDR_{mac,j}$ *(pp/ml/cl)**‡	Mature macrophage depletion rate	0/0/0	10^9 cells/hr	–
CL_{apop}	Apoptotic clearance time constant	1.5	hr	Calculated

*indicates dynamic parameters; initial value shown† *pp/ml/cl*: periportal/midlobular/centrilobular zones of the liver
‡indicates parameters that are used in macrophage depletion experiments; parameter values change from listed values to replicate experimental results§Parameter values were either taken from literature with references listed, calculated, or set to zero for future model expansion.

Table 2. LSEC life cycle parameter values.

PARAMETER	DESCRIPTION	MOUSE VALUE	UNITS	SOURCES§
MR_{lsec}	LSEC maturation rate	1	1/hr	Calculated
$PR_{lsec,j}$ *(pp/ml/cl)**†	LSEC proliferation rate	2.8e-4/2.8e-4/2.8e-4	1/hr	114–116
$AR_{lsec,j}$ *(pp/ml/cl)**	LSEC apoptotic rate	2.8e-4/2.8e-4/2.8e-4	1/hr	Calculated
γ_{lsec}	Rate of mitosis for LSECs	0.042	1/hr	117

*indicates dynamic parameters; initial value shown†*pp/ml/cl*: periportal/midlobular/centrilobular zones of the liver
§Parameter values were either taken from literature with references listed, calculated, or set to zero for future model expansion.

macrophages[55]. It should be noted that while acHMGB1 also acts as a DAMP, it is a distinct molecular entity from the HMGB1 released by necrotic hepatocytes because of the post-translational modification[55]. IL-10 is secreted by activated macrophages, and HGF is produced by activated LSECs[56,57]. In addition to the activation signal, there is also regulation of mediators, *e.g.*, IL-10 downregulation of TNF-α synthesis[58], which will be discussed below. Rates of mediator production are determined by the following set of equations:

Macrophage TNF-α

$$TNF_{prod,mac} = \frac{TNF_{signal,mac}^{TNF_{n,mac}} TNF_{V_{max},mac}}{TNF_{K_m,mac}^{TNF_{n,mac}} + TNF_{signal,mac}^{TNF_{n,mac}}} \quad (10)$$

LSEC TNF-α

$$TNF_{prod,lsec} = \frac{TNF_{signal,lsec}^{TNF_{n,lsec}} TNF_{V_{max},lsec}}{TNF_{K_m,lsec}^{TNF_{n,lsec}} + TNF_{signal,lsec}^{TNF_{n,lsec}}} \quad (11)$$

Macrophage acetylated HMGB1

$$acHMGB1_{prod} = \frac{acHMGB1_{signal}^{acHMGB1_n} acHMGB_{V_{max}}}{acHMGB_{K_m}^{acHMGB_n} + acHMGB_{signal}^{acHMGB_n}} \quad (12)$$

Macrophage IL-10

$$IL10_{prod} = \frac{IL10_{signal}^{IL10_n} IL10_{V_{max}}}{IL10_{K_m}^{IL10_n} + IL10_{signal}^{IL10_n}} \quad (13)$$

The LSEC HGF

$$HGF_{prod} = \frac{HGF_{signal}^{HGF_n} HGF_{V_{max}}}{HGF_{K_m}^{HGF_n} + HGF_{signal}^{HGF_n}} \quad (14)$$

where the subscripts *prod* and *signal* indicate a particular mediator's production and production signal, respectively, and n, V_{max}, and K_m are the parameters of the Hill function describing mediator production. The extra subscripts found in $TNF_{prod,mac}$

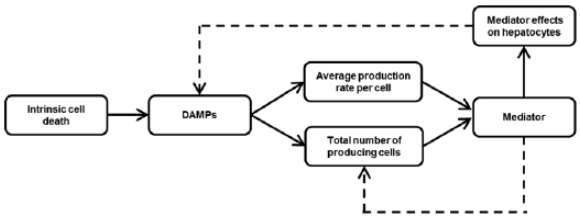

Figure 3. Schematic for mediator production by liver macrophages or liver sinusoidal endothelial cells (LSECs) in DILIsym. Macrophages or LSECs are activated by damage associated molecular pattern (DAMP) molecules released by hepatocytes. Mediator production is a function or a production rate per cell and the total number of activated cells. The latter allows for changes in the size of the cell population to influence mediator production. Mediators may regulate mediator production or act directly on hepatocytes, which may feedback on the instigating DAMP signal. Solid arrows depict the relatively straightforward path from initiation. Dashed arrows depict feedback loops.

and $TNF_{prod,lsec}$ indicate whether the production of TNF-α is regulated by macrophages (*mac*) or LSECS (*lsec*). In addition to the regulated rate of production, total mediator output is also determined by the number of activated cells. This allows the representation to accommodate increased macrophage numbers (Figure 3).

In the model, mediator production parameter values were either derived from the literature or optimized to plasma mediator levels following APAP administration (Table 3).

The aforementioned mediators have effects on the regulation of mediator production, activation of immune cells, and regulation of the hepatocyte life cycle. More specifically, HMGB1 activates liver macrophages and LSECs[53,59]. TNF-α, an extensively studied pleiotropic molecule, can induce hepatocyte necroptosis (*i.e.*, a regulated form of necrosis), apoptosis, survival, or proliferation[38,39]. HMGB1 and TNF-α also stimulate immune cell recruitment, which is supported by data demonstrating that both upregulate adhesion molecules[53,60,61]. In DILIsym, the cellular response to TNF-α is governed by a series of checkpoints that consider the energetic state of the hepatocytes (described in more detail below). TNF-α upregulates its own production, as well as production of IL-10 and acetylated HMGB1[62–65]. TNF-α also upregulates HGF production, which is a simplification. Data suggest that LSEC HGF production is positively regulated by vascular endothelial growth factor (VEGF), where macrophages are a cellular source of VEGF[66,67]. VEGF is not included in the initial representation but could be added. HMGB1 upregulates the production of IL-10, TNF-α, and acetylated HMGB1. In contrast, IL-10 downregulates TNF-α and acetylated HMGB1 production[58]. HGF and TNF-α stimulate hepatocyte proliferation[68–70].

Mediator effect parameter values were either derived from the literature or optimized to plasma mediator levels or macrophage mediator levels following APAP administration (Table 4).

Examples of Modelling Biological Complexity. HMGB1 and TNF-α may be used to illustrate some of the biological complexity in what is understood of molecules thought to be involved in the DILI-related innate immune response.

HMGB1. Alternate redox states or post-translational modifications of HMGB1 have been described, and the detection of these different forms in the blood may provide information on underlying cellular processes in DILI. More specifically, there are three forms of HMGB1 that depend on redox state of three sulfydryl groups which in turn depends on the state of the cell from which HMGB1 is released: a fully reduced form having chemoattractant activity, a disulphide form with a bond between cysteine 23 and 45 having cytokine-inducing activity, and a sulfonyl form of HMGB1 having neither of these pro-inflammatory activities, have been described[24]. The lack of pro-inflammatory activity in the sulfonyl form is consistent with studies on apoptosis, demonstrating that caspase-dependent oxidized HMGB1 contributed to the induction of tolerance[71]. HMGB1 can interact with a number of receptors including TLR2 and TLR4 as well as receptor for advanced glycation end-products (RAGE). It can also bind proteins such as cytokines and chemokines to increase their activity[72].

In DILIsym, hepatocyte necrosis results in the release of a reduced form of HMGB1, which is characterized by cytokine-inducing and immune cell recruitment activity; in contrast, hepatocyte apoptosis results in the release of an oxidized form of HMGB1, which can be detected but is not active:

Active HMGB1 release from necrotic hepatocytes

$$\frac{dH_{act}}{dt} = \eta\lambda - \kappa H_{act} \tag{15}$$

Inactive HMGB1 release from apoptotic hepatocytes

$$\frac{dH_{inact}}{dt} = \lambda \sum_{j=\{pp,\mathbf{ml},cl\}} \rho_j - \xi_j \begin{pmatrix} \mu_j HC_{young,j} \\ +\nu_j HC_{mat,j} \end{pmatrix} - \kappa H_{inact} \tag{16}$$

where H_{act} represents the active non-acetylated HMGB1 release from necrotic hepatocytes and H_{inact} the inactive non-acetylated HMGB1 release from apoptotic hepatocytes. Parameters η, λ, and κ are the hepatocyte necrotic flux, the passive release rate of HMGB1 from necrotic cells, and the transfer rate of HMGB1 from liver to serum. Apoptotic parameters ρ_j, μ_j, ν_j, and ξ_j are the apoptotic flux, the apoptosis rate for young hepatocytes, the apoptosis rate for mature hepatocytes, and the fraction of apoptotic hepatocytes undergoing secondary necrosis, respectively, in zone *j* of the liver. The populations of young and mature hepatocytes in each zone is denoted by $HC_{young,j}$ and $HC_{mat,j}$.

Beyond redox states, acetylated (or hyper-acetylated) HMGB1 *vs.* non-acetylated (or hypo-acetylated) forms have been characterized, where the former is synthesized and secreted by activated macrophages, while the latter is passively released by necrotic cells[55]. Acetylated HMGB1 is a putative biomarker for involvement of the immune response and has been associated with worse prognosis in APAP overdose

Table 3. Mediator parameter values.

PARAMETER	DESCRIPTION	MOUSE VALUE	UNITS	SOURCES§
$TNF_{n,mac}$	Hill parameter for TNF production regulated by macrophages	3	dimensionless	Calculated
$TNF_{Vmax,mac}$	V_{max} parameter for TNF production regulated by macrophages	20000	pg/hr/10^9 cells	78,116–118
$TNF_{Km,mac}$	K_m parameter for TNF production regulated by macrophages	25	dimensionless	Calculated
$TNF_{n,lsec}$	Hill parameter for TNF production regulated by LSECs	3	dimensionless	Calculated
$TNF_{Vmax,lsec}$	V_{max} parameter for TNF production regulated by LSECs	1500	pg/hr/10^9 cells	52,121
$TNF_{Km,lsec}$	K_m parameter for TNF production regulated by LSECs	25	dimensionless	Calculated
$acHMGB1_n$	Hill parameter for HMGB1 production	3	dimensionless	Calculated
$acHMBG1_{Vmax}$	V_{max} parameter for HMGB1 production	50	pg/hr/10^9 cells	25,122,123
$acHMGB1_{Km}$	K_m parameter for HMGB1 production	25	dimensionless	Calculated
$IL10_n$	Hill parameter for IL-10 production	3	dimensionless	Calculated
$IL10_{Vmax}$	V_{max} parameter for IL-10 production	1500	pg/hr/10^9 cells	75,76
$IL10_{Km}$	K_m parameter for IL-10 production	25	dimensionless	Calculated
HGF_n	Hill parameter for HGF production	3	dimensionless	Calculated
HGF_{Vmax}	V_{max} parameter for HGF production	900	pg/hr/10^9 cells	124,125
HGF_{Km}	K_m parameter for HGF production	25	dimensionless	Calculated

§Parameter values were either taken from literature with references listed, calculated, or set to zero for future model expansion

Table 4. HMGB1 release parameter values.

PARAMETERS	DESCRIPTION	MOUSE VALUES	UNITS	SOURCES§
ρ_j *(pp/ml/cl)**†	Apoptotic flux	3.6e-6/2.1e-6/7.1e-7	10^9 cells/hr	126
μ_j *(pp/ml/cl)*	Apoptosis rate for young HCs	0/0/0	1/hr	–
ν_j *(pp/ml/cl)*	Apoptosis rate for mature HCs	3.5e-5/3.5e-5/3.5e-5	1/hr	28, 124–126
ξ_j *(pp/ml/cl)**	Fraction of apoptotic HCs undergoing secondary necrosis‡	0/0/0	dimensionless	–
η*	HC necrotic flux	0	10^9 cells/hr	–
λ	Passive release of HMGB1 from necrotic cells	11333	ng/10^9 cells	130,131
κ	Transfer rate of HMGB1 from liver to serum	90000	1/hr	Calculated

*indicates dynamic parameters; initial value shown
†*pp/ml/cl*: periportal/midlobular/centrilobular zones of the liver
‡apoptotic cells are assumed to be efficiently cleared, *i.e.*, no secondary necrosis, under homeostatic conditions§Parameter values were either taken from literature with references listed, calculated, or set to zero for future model expansion.

patients[26]. In DILIsym, non-acetylated HMGB1 is produced by dying hepatocytes, while acetylated HMGB1 is produced by activated macrophages (see equation 12).

TNF-α. TNF-α is a well-established pleiotropic cytokine, with effects ranging from cell proliferation and survival to apoptosis to necroptosis[38]. Despite the broad acceptance of these divergent behaviours, there is no common data set in which all of these behaviours have been characterized. Thus, there is a need to synthesize data and mechanistic interpretation across multiple data sets to arrive at a cohesive representation.

For DILIsym, the addition of detailed signalling pathways would result in more parameters than could be reasonably constrained with the available data, and the decision was made to seek a proxy. Data were identified that revealed intracellular ATP as a regulator in the cell fate decision to undergo apoptosis *vs.* necrosis[73]. More specifically, Leist et al. simultaneously measured intracellular ATP, apoptosis, and necrosis in cells

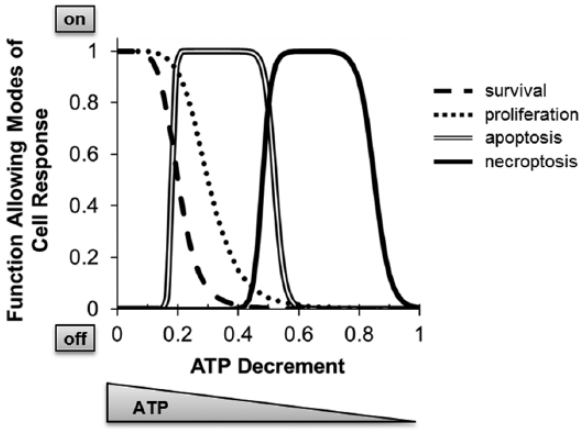

Figure 4. Schematic for the regulation of alternate hepatocyte responses to TNF-α in DILIsym. Adenosine triphosphate (ATP) levels are used as a proxy for cell health or stress. In ATP-replete hepatocytes or with a modest decrement, TNF-α induces a survival signal (dashed line) or proliferative signal (dotted line). In moderately stressed hepatocytes, TNF-α can initiate a caspase-mediated apoptotic pathway (double line). In more severely stressed hepatocytes, TNF-α can induce programmed necrosis or necro-apoptosis (solid line).

cultured with various pharmacologic agents that deplete ATP or induce cell death. Their time and dose-dependent data illustrate that ATP depletion switches the mode of cell death from apoptosis to necrosis. Their data are based on T cells (not hepatocytes) and Fas signalling (not TNF-α receptor signalling), but the relationship was hypothesized to be generalizable to other cell types and other death receptors. The general relationship has been included and extended within DILIsym to establish regimes of TNF-α response, where ATP-replete cells will survive or proliferate; modestly ATP-depleted cells will undergo apoptosis; more severely ATP-depleted cells will undergo necroptosis; and at extreme levels of ATP depletion, necrosis proceeds without need for additional signalling by TNF-α or other inducers of cell death (Figure 4).

Integration

Once the immune equations were generated and populated with steady-state parameter values, the sub-model was integrated to accept DILIsym input values. Particularly, APAP-induced hepatocyte necrosis elevates simulated HMGB1, which is the key input for initial activation of immune cells. Fortunately, there are detailed kinetic studies of HMGB1 elevation following APAP overdose in mice[25]. Notably, HMGB1 levels were elevated for at least 15 hours following APAP administration, suggesting a similar duration of hepatocyte necrosis. While it's likely that early hepatocyte necrosis is due to intrinsic drug-related toxicity, it's possible that later necrosis might include a contribution from immune cells. This hypothesis is supported by the observation that acetylated HMGB1 levels are elevated as early as five hours following APAP administration[25], supporting a putative role for macrophage activation in the overall response.

The integration phase also accommodates the dynamic calculation of immune effects on hepatocytes. Optimization during the integration phase includes the refinement of parameter values to provide an integrated mouse APAP response aligned with the majority of available data. More specifically, simulated APAP overdose leads to elevations in HMGB1 that are comparable to measured data, including both total HMGB1 which largely reflects hepatocyte death and acetylated HMGB1 reflecting macrophage activation (Figure 5a and b). Activation of liver macrophages and LSECs by HMGB1 leads to cellular activation and production of TNF-α (Figure 5c). IL-10 generally acts as a regulatory or inhibitory cytokine, and is generally produced later than TNF-α[74]. Interestingly, the available IL-10 data did not clearly indicate a delayed dynamic, but this might be due to a relatively sparse data set[75,76]. Since IL-10 inhibits TNF-α production, we postulated that peak IL-10 production activity occurs later, which is permissive for early elevations in TNF-α (Figure 5d). The inflammatory mediators also stimulate monocyte recruitment, which leads to expansion of the simulated macrophage population, where macrophage accumulation follows the zonal pattern of damage, *i.e.*, preferential accumulation in the centrilobular zone (Figure 5e). Finally, several reports on the effects of TNF-α on DILI were combined to consider the relationship between APAP dose and TNF-α. The response was generally aligned to no or minimal response below 300 mg/kg and response at doses greater than or equal to 300 mg/kg (Figure 5f). Notably, measurement timing influences the level of TNF-α. This is particularly evident for simulation of 450 mg/kg, where death of the simulated mouse limits the degree of inflammation achieved.

Overall, the mouse APAP simulations include an innate immune response that remains consistent with more liver-centric data comparisons, *e.g.*, ALT, liver mass, ATP, glutathione (Supplement 1).

Species Translation of Parameter Values. As previously mentioned, the availability of mouse immune data, including time course data, was much greater than data for rats or humans and accounted for the decision to start with a mouse representation. With a mouse representation that aligned with the majority of the measured data as described above, corresponding rat and human parameter values could be derived.

Some rat and human data (*e.g.*, circulating monocyte concentrations) were available to guide the selection of rat and human parameter values. Where no species-specific data were available to guide parameter changes, parameter values remained identical to mouse parameter values. Rat and human simulations were then conducted and compared against measured data. In some instances, additional parameter value refinement was required based on mediator levels, time courses, and effects. To facilitate the identification of species differences, the refinements were designated as scalar multipliers. The resultant rat and human parameter values are listed in Tables 5 and 6, respectively.

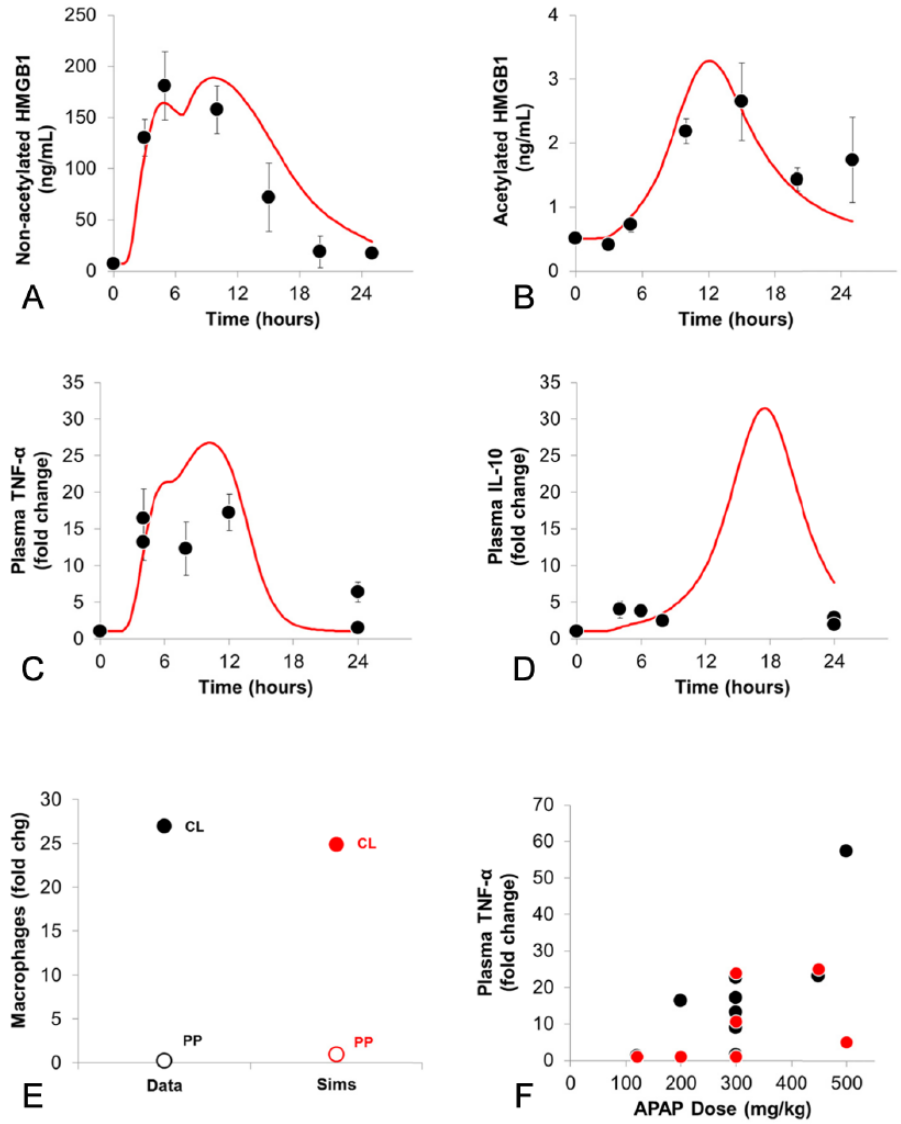

Figure 5. Comparison between measured data (mean ± SD or mean fold change ± normalized error) and simulation results from mice administered a single dose of APAP. In the measured data, samples were collected at various time points after APAP administration and measured for various analytes: a) non-acetylated HMGB1[25], b) acetylated HMGB1[25], c) TNF-α[75,118–120], d) IL-10[75,76]. In e) the change in centrilobular (CL) and periportal (PP) liver macrophages 48 hours post-APAP was determined from CD11b staining in liver sections[37]. In f) measured data and simulation results for TNF-α[75,85,87,118–120,153,154] are compared from mice administered different doses of APAP. Notably, published studies also vary by mouse strain and time of sample collection. Simulation results reflect the published APAP dose and time of sample collection, but no parameter value changes were made to accommodate potential differences in mouse strain.

The few reports of plasma TNF-α levels following APAP administration in rats show widely disparate degrees of elevation, likely reflecting both differences in methodology and natural variation[77,78]. Varying the simulated APAP dose illustrates that simulated TNF-α can cover a range of response though not as extensive as that reported in rats treated with APAP (Figure 6). Expanding the comparator data set to include TNF-α data from other rat liver inflammation experimental models suggests the range of simulated TNF-α is consistent with the majority of data sets (Supplement 2). Other rat data comparisons rely entirely on non-APAP data and are shown in Supplement 2.

Several papers have reported circulating mediator levels in patients with liver injury (predominantly due to APAP overdose) or disease[79–83]. Thus, data comparisons were possible for TNF-α and IL-10 (Figure 7a and b). Additionally, biopsy data could be leveraged to compare simulated macrophage accumulation against measured data (Figure 7c). Simulated mediator levels and cellular accumulation results across a range of APAP doses were generally consistent with the measured data. Within the human data set, there were also time course total and acetylated HMGB1 data from a small number of APAP overdose patients[26]. Interestingly, this study identified an association between higher acetylated HMGB1 levels and poorer patient outcomes (*i.e.*, death or liver transplant). In DILIsym, this may be evaluated by simulating lower overdoses that result in survival and higher overdoses causing severe liver injury that could result in death. A comparison of simulation results and the HMGB1

Table 5. Rat parameter values.

PARAMETER	DESCRIPTION	RAT VALUE	UNITS	SOURCES[§]
Macrophage life cycle parameters				
α	Influx of monocytes from bone marrow to circulation	1.1e-5	10^9 cells/hr/mL blood	132
β	Rate constant representing non-liver recruitment of macrophages	0.0125	1/hr	100(p19)
γ_{mac}	Rate of mitosis for macrophages	0.0416	1/hr	101–104
BV	Blood volume	18.5	mL	105
$RR_{mac,j}$ (pp/ml/cl)*†	Macrophage recruitment rate	0.0097/0.0044/9.7e-4	1/hr	100,106,107
$MR_{mac,j}$ (pp/ml/cl)*	Macrophage maturation rate	0.008/0.008/0.008	1/hr	92
$PR_{mac,j}$ (pp/ml/cl)*	Macrophage proliferation rate	3.6e-4/3.6e-4/3.6e-4	1/hr	98,106–111
$AR_{mac,j}$ (pp/ml/cl)*	Macrophage apoptotic rate	0.0014/0.0014/0.0014	1/hr	Calculated
$IDR_{mac,j}$ (pp/ml/cl)* ‡	Immature macrophage depletion rate	0/0/0	10^9 cells/hr	–
$MDR_{mac,j}$ (pp/ml/cl)*‡	Mature macrophage depletion rate	0/0/0	10^9 cells/hr	–
CL_{apop}	Apoptotic clearance time constant	1.5	hr	Calculated
LSEC life cycle parameters				
MR_{lsec}	LSEC maturation rate	1	1/hr	Calculated
$PR_{lsec,j}$	LSEC proliferation rate	9.3e-5/9.3e-5/9.3e-5	1/hr	114–116
$AR_{lsec,j}$	LSEC apoptotic rate	9.3e-5/9.3e-5/9.3e-5	1/hr	Calculated
γ_{lsec}	Rate of mitosis for LSECs	0.042	1/hr	117
Mediator parameters				
$TNF_{n,mac}$	Hill parameter for TNF production regulated by macrophages	3	dimensionless	Calculated
$TNF_{Vmax,mac}$	V_{max} parameter for TNF production regulated by macrophages	670000	pg/hr/10^9 cells	80,81,127,128
$TNF_{Km,mac}$	K_m parameter for TNF production regulated by macrophages	25	dimensionless	Calculated
$TNF_{n,lsec}$	Hill parameter for TNF production regulated by LSECs	3	dimensionless	Calculated
$TNF_{Vmax,lsec}$	V_{max} parameter for TNF production regulated by LSECs	50000	pg/hr/10^9 cells	52,121
$TNF_{Km,lsec}$	K_m parameter for TNF production regulated by LSECs	25	dimensionless	Calculated
$acHMGB1_n$	Hill parameter for HMGB1 production	3	dimensionless	Calculated
$acHMBG1_{Vmax}$	V_{max} parameter for HMGB1 production	5	pg/hr/10^9 cells	135–141
$acHMGB1_{Km}$	K_m parameter for HMGB1 production	25	dimensionless	Calculated
$IL10_n$	Hill parameter for IL-10 production	3	dimensionless	Calculated
$IL10_{Vmax}$	V_{max} parameter for IL-10 production	10000	pg/hr/10^9 cells	134,142
$IL10_{Km}$	K_m parameter for IL-10 production	25	dimensionless	Calculated
HGF_n	Hill parameter for HGF production	3	dimensionless	Calculated
HGF_{Vmax}	V_{max} parameter for HGF production	16000	pg/hr/10^9 cells	143–145

Table 5. (Continued)

PARAMETER	DESCRIPTION	RAT VALUE	UNITS	SOURCES§
HGF_{Km}	K_m parameter for HGF production	25	dimensionless	Calculated
HMGB1 release parameters				
ρ_j *(pp/ml/cl)**	Apoptotic flux	2.1e-4/1.2e-3/4.1e-5	10^9 cells/hr	126
μ_j *(pp/ml/cl)*	Apoptosis rate for young HCs	0/0/0	1/hr	–
ν_j *(pp/ml/cl)*	Apoptosis rate for mature HCs	3.5e-5/3.5e-4/3.5e-4	1/hr	28, 124–126
ξ_j *(pp/ml/cl)**	Fraction of apoptotic HCs undergoing secondary necrosis	0/0/0	dimensionless	–
η^*	HC necrotic flux	0	10^9 cells/hr	–
λ	Passive release of HMGB1 from necrotic cells	10000	ng/10^9 cells	130,131
κ	Transfer rate of HMGB1 from liver to serum	90000	1/hr	Calculated

*indicates dynamic parameters; initial value shown† *pp/ml/cl*: periportal/midlobular/centrilobular zones of the liver
‡indicates parameters that are used in macrophage depletion experiments; parameter values change from listed values to replicate experimental results§Parameter values were either taken from literature with references listed, calculated, or set to zero for future model expansion.

Table 6. Human parameter values.

PARAMETER	DESCRIPTION	HUMAN VALUE	UNITS	SOURCES§
Macrophage life cycle parameters				
α	Influx of monocytes from bone marrow to circulation	8.1e-6	10^9 cells/hr/mL blood	146
β	Rate constant representing non-liver recruitment of macrophages	0.014	1/hr	100(p19)
γ_{mac}	Rate of mitosis for macrophages	0.0416	1/hr	101–104
BV	Blood volume	4881	mL	105
$RR_{mac,j}$ *(pp/ml/cl)*†*	Macrophage recruitment rate	0.004/0.0018/4.0e-4	1/hr	100,106,107
$MR_{mac,j}$ *(pp/ml/cl)**	Macrophage maturation rate	0.008/0.008/0.008	1/hr	92
$PR_{mac,j}$ *(pp/ml/cl)**	Macrophage proliferation rate	3.4e-4/3.4e-4/3.4e-4	1/hr	98,106–111
$AR_{mac,j}$ *(pp/ml/cl)**	Macrophage apoptotic rate	0.0011/0.0011/0.0011	1/hr	Calculated
$IDR_{mac,j}$ *(pp/ml/cl)*‡*	Immature macrophage depletion rate	0/0/0	10^9 cells/hr	–
$MDR_{mac,j}$ *(pp/ml/cl)* *‡	Mature macrophage depletion rate	0/0/0	10^9 cells/hr	–
CL_{apop}	Apoptotic clearance time constant	1.5	hr	Calculated
LSEC life cycle parameters				
MR_{lsec}	LSEC maturation rate	1	1/hr	Calculated
$PR_{lsec,j}$	LSEC proliferation rate	6.3e-5/6.3e-5/6.3e-5	1/hr	114–116
$AR_{lsec,j}$	LSEC apoptotic rate	6.3e-5/6.3e-5/6.3e-5	1/hr	Calculated
γ_{lsec}	Rate of mitosis for LSECs	0.042	1/hr	117
Mediator parameters				
$TNF_{n,mac}$	Hill parameter for TNF production regulated by macrophages	3	dimensionless	Calculated

(Continued)

Table 6. (Continued)

PARAMETER	DESCRIPTION	HUMAN VALUE	UNITS	SOURCES§
$TNF_{Vmax,mac}$	V_{max} parameter for TNF production regulated by macrophages	110000	pg/hr/10^9 cells	79–83
$TNF_{Km,mac}$	K_m parameter for TNF production regulated by macrophages	25	dimensionless	Calculated
$TNF_{n,lsec}$	Hill parameter for TNF production regulated by LSECs	3	dimensionless	Calculated
$TNF_{Vmax,lsec}$	V_{max} parameter for TNF production regulated by LSECs	8200	pg/hr/10^9 cells	52,121
$TNF_{Km,lsec}$	K_m parameter for TNF production regulated by LSECs	25	dimensionless	Calculated
$acHMGB1_n$	Hill parameter for HMGB1 production	3	dimensionless	Calculated
$acHMBG1_{Vmax}$	V_{max} parameter for HMGB1 production	60	pg/hr/10^9 cells	26,147–149
$acHMGB1_{Km}$	K_m parameter for HMGB1 production	25	dimensionless	Calculated
$IL10_n$	Hill parameter for IL-10 production	3	dimensionless	Calculated
$IL10_{Vmax}$	V_{max} parameter for IL-10 production	10000	pg/hr/10^9 cells	[79–83]
$IL10_{Km}$	K_m parameter for IL-10 production	25	dimensionless	Calculated
HGF_n	Hill parameter for HGF production	3	dimensionless	Calculated
HGF_{Vmax}	V_{max} parameter for HGF production	1100	pg/hr/10^9 cells	150(p1),151,152]
HGF_{Km}	K_m parameter for HGF production	25	dimensionless	Calculated
HMGB1 release parameters				
ρ_j *(pp/ml/cl)**	Apoptotic flux	0.019/0.011/0.0037	10^9 cells/hr	126
μ_j *(pp/ml/cl)*	Apoptosis rate for young HCs	0/0/0	1/hr	–
ν_j *(pp/ml/cl)*	Apoptosis rate for mature HCs	1.7e-4/1.7e-4/1.7e-4	1/hr	28, 124–126
ξ_j *(pp/ml/cl)**	Fraction of apoptotic HCs undergoing secondary necrosis	0/0/0	dimensionless	–
η^*	HC necrotic flux	0	10^9 cells/hr	–
λ	Passive release of HMGB1 from necrotic cells	11500	ng/10^9 cells	130,131
κ	Transfer rate of HMGB1 from liver to serum	0.03	1/hr	Calculated

*indicates dynamic parameters; initial value shown† *pp/ml/cl*: periportal/midlobular/centrilobular zones of the liver
‡indicates parameters that can be used in macrophage depletion experiments; such experiments would be exploratory as not corresponding data have been identified
§Parameter values were either taken from literature with references listed, calculated, or set to zero for future model expansion.

data suggests that, in DILIsym, acetylated HMGB1 also associates with poor outcomes (Figure 8). It should be noted that, while these data comparisons are technically considered part of optimization because they are done with APAP overdose, the results are emergent results based on "humanizing" the mouse parameter values. No additional refinement of parameter values was required to reproduce these data.

Qualification

In the qualification phase, compounds can be added or new experimental manipulations can be attempted to characterize and test the behaviours as simulated for innate immune responses in the context of DILI.

Immune-relevant Interventions in Combination with APAP. The simulated innate immune response is by design, generally consistent with the measured data for APAP overdose in mice. Interventions combined with APAP overdose have been investigated experimentally and in DILIsym, including pharmacologic blockade of HMGB1 and TNF-α and pharmacologic depletion of macrophages. Because none of these are DILI compounds, they are represented simply in DILIsym and without detailed pharmacokinetics.

Pharmacologic blockade of HMGB1 effects. The role of HMGB1 as an initiator of immune responses in APAP DILI has been studied via pharmacologic and genetic intervention. The administration of blocking antibodies specific for HMGB1 has the effect of mitigating elevations in pro-inflammatory cytokine levels and ALT, with a corresponding reduction in hepatocyte necrosis[27–29]. Genetic ablation of HMGB1 specifically in hepatocytes has also been shown to be protective[30]. In DILIsym, blockade of hepatocyte HMGB1 is represented as an inhibitory multiplier of plasma HMGB1 concentrations to yield an effective HMGB1 concentration. Level and duration of inhibition can be specified. The simulation results are qualitatively consistent with the net protective effect observed experimentally when abrogating the effect of HMGB1 (Figure 9). Parameter values were not further optimized to obtain this result, suggesting that the representation of HMGB1 as an initiator of an innate response that contributes to injury progression is generally consistent with the system-level behaviour.

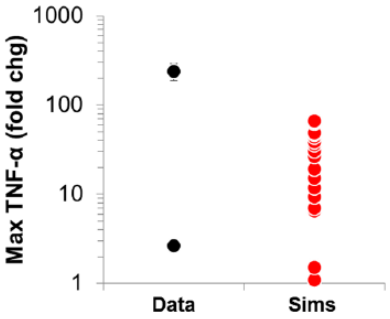

Figure 6. Comparison between TNF-α measured data (mean fold change ± normalized error) and simulation results from rats administered a single dose of APAP. Measured data reflect maximum elevation in TNF-α following APAP doses of 1000 or 1500 mg/kg[77,78]. Simulation results reflect maximum elevation in TNF-α across doses ranging from 900 to 1500 mg/kg. Supplement 2 includes this comparison and additional data from non-APAP liver inflammation models that provide a broader perspective on experimentally observed TNF-α elevations.

Pharmacologic blockade of TNF-α effects. The role of TNF-α has been studied via pharmacologic and genetic intervention for its contributions to APAP DILI. The administration of blocking antibodies specific for TNF-α mitigated elevations in TNF-α and circulating transaminases, with corresponding reduction in hepatocyte necrosis[86–88], although one report was unable to replicate this finding[89] . Genetic ablation of TNF-α receptor 1 subunit was also found to be protective[88] . Separate efforts targeting tumour necrosis factor receptor 1 (TNFR1) or TNF-α and lymphotoxin (LT) found the opposite effect of exaggerated APAP DILI[89,90] Given the pleiotropic nature of TNF-α, it is perhaps not surprising that different methods and different laboratories could yield different but still plausible results. In DILIsym, TNF-α blockade is represented as an inhibitory multiplier of plasma TNF-α concentrations to yield an effective TNF-α concentration. As with the blockade of HMGB1, duration and degree of inhibition are specified. Simulations are generally consistent with the net protective effect observed with pharmacologic inhibition, although greater protection was sometimes observed in the measured data (Figure 10). As no parameter values were modified, this analysis suggested the TNF-α representation was consistent with measured data suggesting TNF-α contributes to injury.

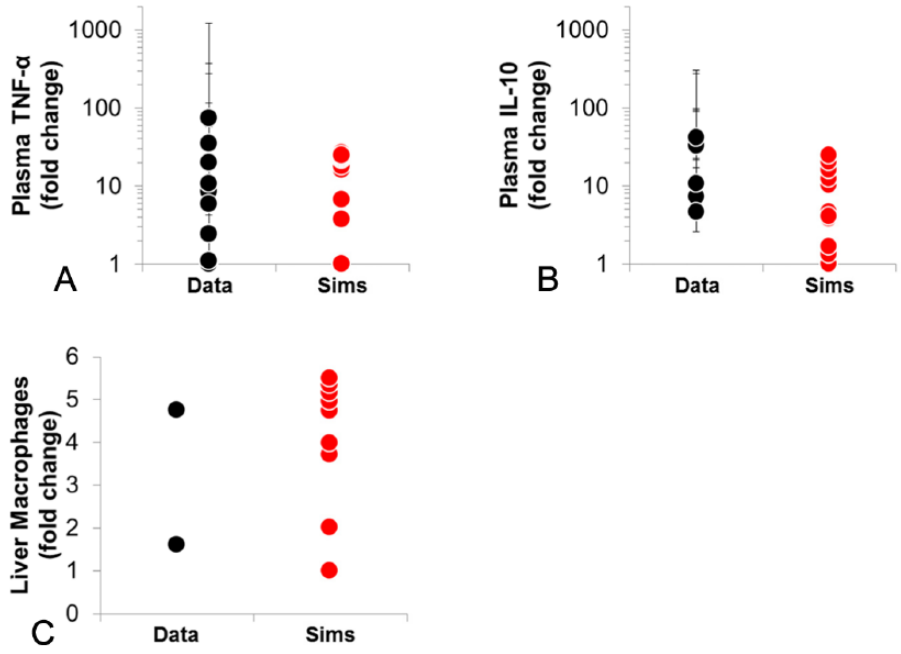

Figure 7. Comparison between measured data (mean fold change ± normalized error) and simulation results from APAP overdose in humans for a) TNF-α[79–83], b) IL-10[79–81], and c) liver macrophages[80]. Measured data reflect a range of response in overdose patients. Simulation results reflect maximum responses to 30-55g APAP overdose.

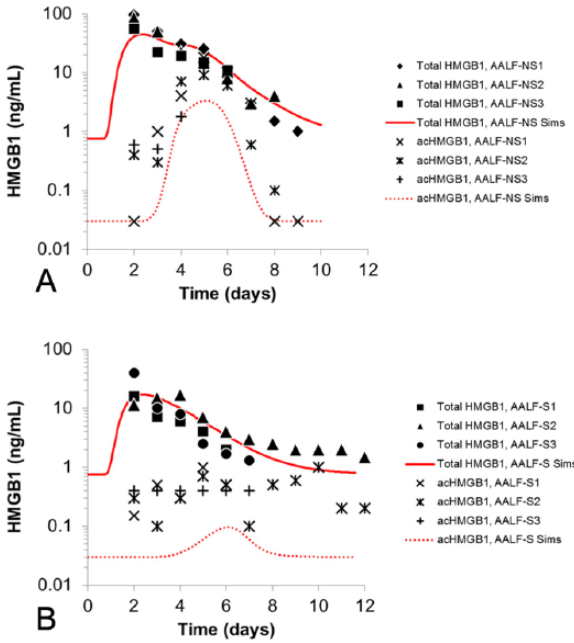

Figure 8. Comparison between measured data and simulation results for HMGB1 from APAP overdose in humans. Total and acetylated HMGB1 were measured in individual patients that were classified as a) non-survivors (*i.e.*, required liver transplant or died) or b) survivors[26] (filled shape symbols for total HMGB1, line symbols for acetylated HMGB1); For comparison, simulations were conducted with a) 52g overdose, and b) 42g overdose (solid red line for total HMGB1, dashed red line for acetylated HMGB1).

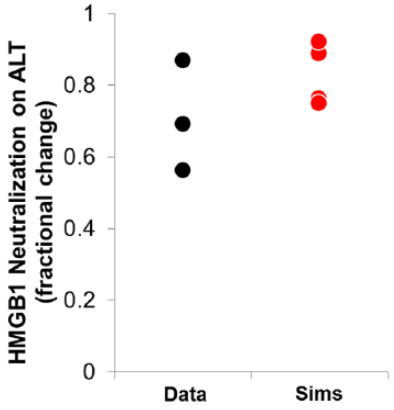

Figure 9. Comparison between measured data[27–29] and simulation results for the effect of HMGB1 neutralization on APAP-induced ALT in mice. In the measured data, mice received an acute dose of APAP, in the absence or presence of neutralizing antibodies to HMGB1. The studies varied with respect to mouse strain, APAP dose, neutralizing antibody, time of antibody administration, and time of sample collection. The fractional changes in the measured ALT response depending on the presence of neutralizing antibody were compared against the fractional changes in simulated maximum ALT response based on blocking simulated HMGB1, using a range of APAP doses (250-400 mg/kg) across the same experimental time interval (6-24 hr).

Pharmacologic depletion of macrophages. Intravenously administered liposome-encapsulated clodronate is taken up by phagocytes and induces apoptosis in these cells[92] . This is a relatively well-accepted method to investigate the role of macrophages, although other phagocytic cells (*e.g.*, monocytes) are also depleted[91]. In mice and rats, liposome-encapsulated clodronate has been used to investigate liver macrophage population dynamics[92,93], and this technique was used in an influential study demonstrating that liver macrophages have a net protective effect in APAP DILI[44]. More specifically, measured alanine aminotransferase (ALT) and histopathology indicated more severe APAP injury following treatment with liposome-encapsulated clodronate. These data have been instrumental in highlighting the potential for ongoing regulatory or regenerative activities, even during acute injury.

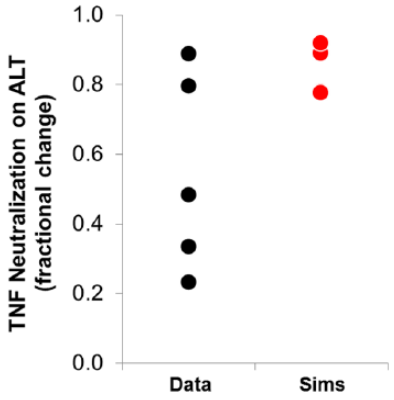

Figure 10. Comparison between measured data[84,86] and simulation results for the effect of TNF-α neutralization on APAP-induced ALT in mice. In the measured data, mice received an acute dose of APAP, in the absence or presence of neutralizing antibodies to TNF-α. The studies varied with respect to mouse strain, APAP dose, neutralizing antibody, time of antibody administration, and time of sample collection. The fractional changes in the measured ALT response depending on the presence of neutralizing antibody were compared against the fractional changes in simulated maximum ALT response based on blocking simulated TNF-α, using a range of APAP doses (250-400 mg/kg) across the same experimental time interval (4-24 hr).

The potential role of macrophages in liver injury has evolved with ongoing investigation. Subsequent studies using clodronate indicated the ALT elevation was more prolonged than the clear histopathological differences[45] or ALT elevations existed in the absence of histopathological differences[46]. Finally, the use of liposome-encapsulated clodronate in CCR2-/- mice, intended to ablate the contribution of both resident and infiltrating macrophages, demonstrated no clodronate-related difference in APAP-induced ALT or histopathological severity relative to liposomal controls[47]. No effect of clodronate on ALT has also been observed in other mouse models[48]. Altogether, these studies suggest that macrophages may not be pivotal in mitigating acute injury, as originally suggested. Instead, the preponderance of data now suggests the absence of macrophages lengthens recovery time, and this may be due to effects of macrophages on the vasculature[47]. Thus, the putative role of macrophages has shifted from an early role in hepatocyte protection through the production of regulatory or pro-regenerative factors to an indirect role in later recovery via vascular effects.

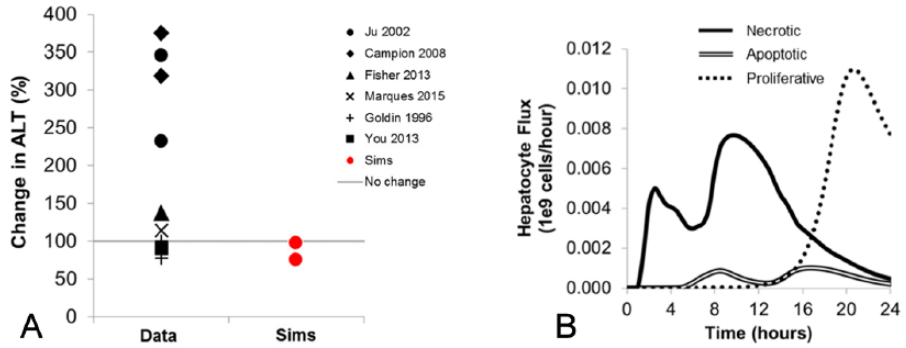

Figure 11. Effects of macrophage depletion. In a) simulation results are compared with mouse measured data for effects of macrophage depletion on APAP-induced ALT[44–48,155] . In the measured data, mice were pre-treated with empty or clodronate-encapsulated liposomes, and then administered an acute dose of APAP. The studies varied with respect to mouse strain, clodronate dose, APAP dose, and time of sample collection. The fractional changes (sometimes >1) in the measured ALT based on macrophage depletion were compared against the fractional changes in simulated maximum ALT response based on the same, using a range of APAP doses (300-500 mg/kg) across the same experimental time interval (6-24 hr). Results in b) show simulated cellular responsiveness of hepatocytes following APAP overdose (300 mg/kg).

In DILIsym, the effect of clodronate on macrophages is represented by increasing macrophage apoptosis, where the absence of macrophages will abrogate the APAP-induced increases in TNF-α and IL-10. The net simulated effect is slightly milder injury, which is not consistent with the majority of the data (Figure 11a). This is not surprising given that, during early stages of acute APAP overdose, many simulated hepatocytes are ATP-depleted and will undergo cell death in response to TNF-α; later, more simulated hepatocytes will have sufficient ATP to proliferate during the hepatocyte recovery phase (Figure 11b). With macrophage depletion, simulated injury is less, which pre-disposes the system towards less proliferation. This illustrates an instance where DILIsym did not reproduce the measured data but points to scenarios that could explain the discrepancy.

One hypothetical explanation is that macrophage depletion may itself exacerbate APAP DILI. An alternative hypothetical explanation is that the current contribution of simulated macrophages to injury progression may be largely due to another cell type, which would allow macrophages to have a greater contribution to regeneration. There are data to support both hypotheses. For the former, a direct effect of macrophage depletion on exacerbation is implicated by the observation of mild liver enzyme elevations following treatment with liposome-encapsulated clodronate alone[94]. For the potential contribution of other cell types, the protection afforded by hepatocyte-specific genetic ablation of HMGB1 has been shown to be associated with neutrophil infiltration[30]. While neutrophils are observed in the liver following toxic doses of APAP, their significance has been controversial, with reports indicating a role in injury progression, while others have shown no effect[41,43,95]. The controversy argued against inclusion of neutrophils in DILIsym initially, but these new genetic ablation data do not suffer some of the weaknesses of earlier datasets and appear to renew the possibility of a neutrophil contribution. Efforts are currently underway to add neutrophils to DILIsym, leveraging the new data, and with the aim of investigating the putative role of neutrophils in injury progression.

Carbon Tetrachloride (CCl_4). Although not a drug, CCl_4 is commonly used to induce acute or chronic liver injury and study potential treatments for DILI[96]. Acute injury results from a single high dose, while chronic injury results from lower and repeated doses. There are similarities to APAP in that CCl_4 is metabolized by P450 enzymes, generates a reactive metabolite, and is thought to induce oxidative stress, although toxicity may also involve mitochondrial dysfunction[97,98]. Additionally, a CCl4-associated innate immune response has been partially characterized in mice and rats.

Acute CCl_4 toxicity has been represented in DILIsym in order to compare simulation results and published data on plasma TNF-α, macrophage accumulation, and response to blocking TNF-α. Simulated CCl_4 comparisons for other measured data (*e.g.*, PK, ALT, ROS) were generally consistent with published reports (Supplement 3), by design. The results demonstrate that simulations are consistent with the range of reported elevations in plasma TNF-α and liver macrophages but that blocking TNF-α results in only modest protection which is quantitatively at odds with the dramatic protection observed experimentally (Figure 12a and b).

It is surprising that simulations are consistent with the degree of inflammation, as defined by TNF-α and macrophages, but inconsistent with the degree of protection afforded by blocking TNF-α, particularly when similar experiments were consistent with protection in APAP hepatotoxicity (Figure 10). The discrepancy stems from a difference in dose-sensitivity. Using mice as an example, APAP hepatotoxicity generally occurs with 200-300 mg/kg dosing. In fact, the majority of publications use 300 mg/kg, and it's relatively rare to find reports where doses greater than 500 mg/kg are administered. In contrast, CCl_4 hepatotoxicity is induced at doses ranging from 10-500 mg/kg. With over an order of magnitude

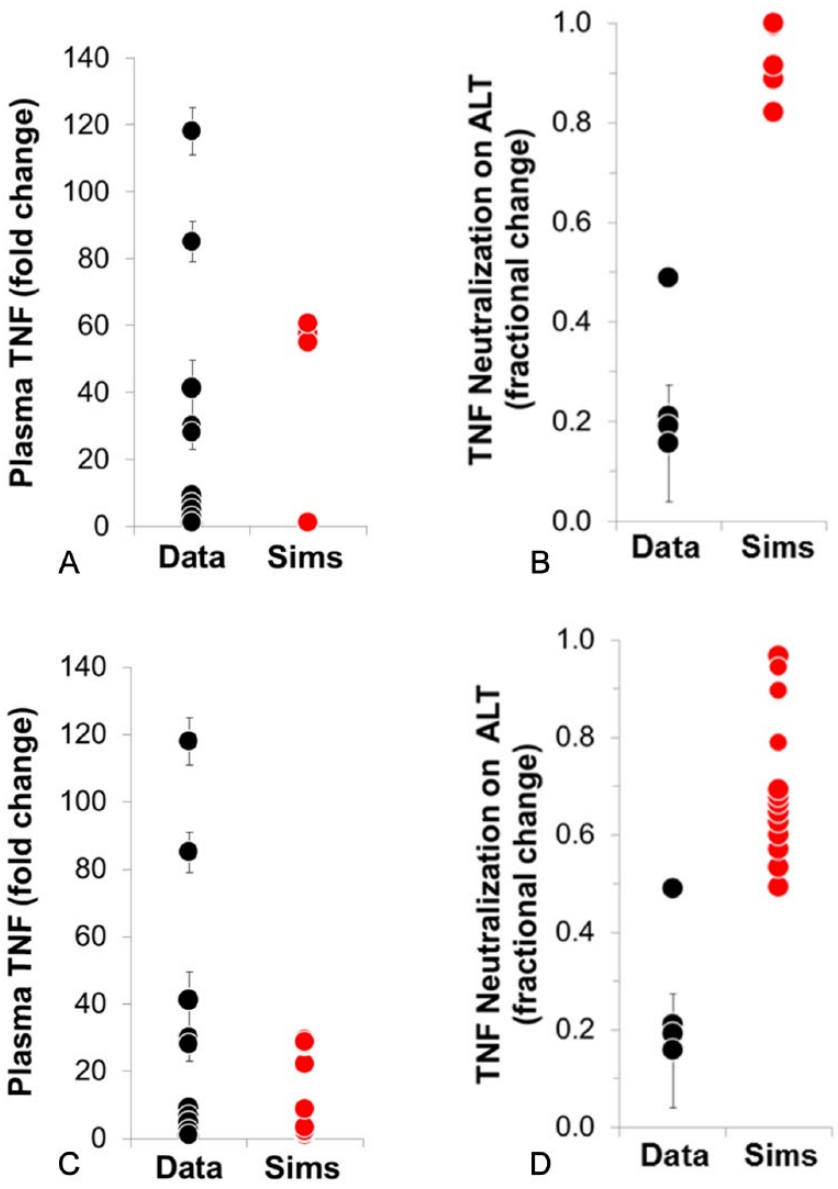

Figure 12. Comparison of mouse measured data and simulation results for CCl_4-induced TNF-α (a,c)[97,156–161] and the effects of TNF-α neutralization on CCl_4-induced ALT elevations (b, d)[162]. In the measured data for a) and c), mice were treated with CCl_4, plasma samples were collected and analyzed for TNF-α. In the measured data for b) and d), mice were treated with CCl_4 in the absence or presence of neutralizing antibodies to TNF-α; serum samples were analyzed for ALT. The studies varied with respect to mouse strain, CCl_4 dose, neutralizing antibody, time of antibody administration, and time of sample collection. For a) and c), elevated TNF-α following CCl_4 administration is compared between measured data (mean fold change ± normalized error) and simulation results (fold change). For b) and d), the fractional changes in the measured ALT response based on the presence of neutralizing antibody were compared against the fractional changes in simulated maximum ALT response based on blocking simulated TNF-α. Simulations use a range of CCl_4 doses (1-1000 mg/kg) across an experimental time interval consistent with the published data (24 hr for plasma TNF-α, 48 hr for TNF-α neutralization). Results in a) and b) show the initial comparison, while c) and d) show the comparison after further refining DILIsym.

dose range, much of the simulated injury was occurring without need for immune amplification. The immune contribution appears at relatively high doses and marginally impacted the degree of injury.

Although there is widespread support within the scientific community for a potential contribution of innate immune responses to DILI, quantitative data characterizing the response are relatively sparse. To improve the DILIsym representation, the initial CCl_4 simulation results have been used to inform changes to parameter values and model structure characterizing the relationship between DAMPs and immune cell activation. Initially, the equations for the production of mediators (eqs. 10-14 above) also included an additional logical value termed the inflammation state, which was modulated with specific threshold levels of DAMPs or TNF-α (DILIsym v2A). The CCl_4 representation demonstrated that mediator production should be a continuous function controlled by mediator levels, without the additional on/off control element. Parameter value changes also accompanied the structure changes (Table 7). With the updated parameter values and equation design,

Table 7. Parameter values changed with CCl_4 re-optimization.

PARAMETER	DESCRIPTION	SPECIES	ORIGINAL VALUE	FINAL VALUE	UNITS
$TNF_{Vmax,mac}$	V_{max} parameter for TNF production regulated by macrophages	Mouse	*10000*	20000	pg/hr/10^9 cells
$TNF_{Vmax,mac}$	V_{max} parameter for TNF production regulated by macrophages	Human	*85800*	110000	pg/hr/10^9 cells
$TNF_{Vmax,lsec}$	V_{max} parameter for TNF production regulated by LSECs	Mouse	*12000*	1500	pg/hr/10^9 cells
$TNF_{Vmax,lsec}$	V_{max} parameter for TNF production regulated by LSECs	Human	*6400*	8200	pg/hr/10^9 cells
$IL10_{Vmax}$	V_{max} parameter for IL-10 production	Mouse	*1833*	1500	pg/hr/10^9 cells
$IL10_{Vmax}$	V_{max} parameter for IL-10 production	Human	*30000*	10000	pg/hr/10^9 cells
$IL10_{Vmax}$	V_{max} parameter for IL-10 production	Rat	*16800*	10000	pg/hr/10^9 cells

immune cell activation and injury amplification occurs at lower levels of injury. CCl_4-induced elevations in TNF-α still cover much of the reported range, but blocking TNF-α is more effective and better aligned with the experimental data (Figure 12c and d). Some measured responses are still greater than the simulated responses; and this may be due to as yet unrepresented activity of TNF-α although specific supporting data have not been identified. Finally, the parameter changes made in Table 7 did not substantively alter the other model behaviours.

Thus, the exercise in adding CCl_4 to test the representation successfully reproduced innate immune indicators in injury and uncovered a quantitative discrepancy in the contribution to injury which was not apparent when evaluating APAP alone. The exercise highlights the need for additional compounds to further test the representation.

Discussion

A mechanistic representation of an innate immune response, activated by DAMPs, and largely mediated by macrophages, has been developed and integrated in DILIsym. By design, the simulated response to toxic doses of APAP in mice is consistent with the majority of published data. The parameter values optimized to the available mouse literature have been translated and compared with the available rat and human data, and these are also consistent with the majority of the published data. The equations, parameter values, and associated documentation for the innate immune sub-model gathers the publicly available data and understanding of this biology into a common (and extensible) framework that can be used to test hypotheses on the innate immune response in DILI.

The contribution of the innate immune response to APAP DILI has been investigated in DILIsym with the relatively simple representation of reducing the amount of HMGB1 available, reducing the amount of TNF-α available, or by inducing apoptosis in hepatic macrophages. Blocking HMGB1 or TNF-α were found to reduce inflammation and the severity of liver injury, qualitatively consistent with the measured data. Macrophage depletion was also found to reduce inflammation and liver injury, which is not consistent with the majority of the measured data. Interestingly though, the interpretation of macrophage activity based on the measured data has evolved from the initial findings and is now more in line with a pro-regenerative function in DILIsym macrophages. More specifically, early measured data seemed to suggest that macrophage protective function could manifest early, offsetting the severity of injury. In DILIsym, this would require TNF-α protective function or HGF proliferative activity when hepatocytes are ATP-depleted, which would be difficult to reconcile with the current representation. In contrast, more recent and accumulating measured data seem to suggest that the absence of macrophages minimally alters or does not alter the severity of injury; rather, macrophages influence recovery. During the recovery phase, hepatocyte ATP levels are much improved, which would be consistent with the timing of protective macrophage function as present in DILIsym.

The simulated innate immune response is dynamically integrated within DILIsym, such that, if DAMPs are produced, an immune response can result in a compound-independent manner. Thus, compounds that induce hepatocyte necrosis via reactive metabolite, oxidative stress, bile acid accumulation, and/or mitochondrial dysfunction, all have the potential to induce an innate immune response. The successful simulation of hepatotoxicity due to compounds not used to optimize immune parameters[15,18] provides indirect support that the immune system representation is reasonable within the whole DILI context. These other compounds also provide the opportunity to design experiments to test for the predicted innate immune response. Consideration of these studies is underway.

Although the modelled innate immune response is consistent with much of the data, there are areas for improvement besides the representation of the effects of macrophage depletion. One area would be to gather additional time course data on circulating levels of TNF-α, IL-10, and HGF to improve confidence in our understanding of the true dynamic profile. A related pursuit

might be to gather time course data on other mediators of interest. Many functions are controlled by multiple mediators, which provide a measure of redundancy, but also flexibility as mediators may vary by cellular source, regulation of synthesis, and/or receptor distribution. Other immune cell populations, *e.g.*, neutrophils, NK cells, dendritic cells, could be added. For neutrophils and NK cells, there are some data describing these cells in mouse APAP DILI, but it might also be prudent to add other DILI compounds for which they've been described. Even for the current representation, adding compounds for further testing and characterization would be desirable. Finally, the current representation sets the stage for, but does not yet address, the pressing problem of DILI mediated by the adaptive immune response. Compound-mediated hepatocellular stress, DAMP release, DAMP-activated immune cells, and pro-inflammatory, as well as regulatory, mediator production are all likely contributors to an adaptive immune response. It can be argued that the addition of T cells to the model, including their differentiation, regulation, and effector activity, would be required to realize the true value of an immune representation in DILIsym.

In summary, DILI remains a significant concern in drug development and utilization. We have described DILIsym, a mechanistic mathematical model which simulates the effects of *in vivo* drug exposure on putative mechanisms of hepatotoxicity, thus providing biological context for the prediction of DILI. Inflammation is widely believed to contribute to DILI events, although relatively little mechanistic data are available. The QST modelling approach adopted by DILIsym provides a means to systematically investigate immune responses, identify data gaps, and prioritize research. As a starting point, DILIsym has incorporated an innate immune response and, in so doing, has gathered the available data into a common framework that extends across pre-clinical species and to humans. Comparison of simulation results and measured data indicate many places where this relatively simple representation is consistent and a few places where mismatches argue for additional refinement. We present DILIsym as an important new tool for the assessment of compound liver safety and for the investigation of contributions by an innate immune response, and with the potential to extend to the challenge of adaptive immune mediated DILI.

Acknowledgements

The authors would like to acknowledge the members of the DILI-sim Initiative for their support in the development of the DILIsym model. More information on the DILI-sim Initiative can be found at www.dilisym.com.

Author Contributions

Conceived and designed the experiments: LKMS, SQS, DSP, PBW, BAH. Analysed the data: LKMS, CB, SQS, DSP, BAH. Wrote the first draft of the manuscript: LKMS. Contributed to the writing of the manuscript: CB, BAH. Agree with manuscript results and conclusions: LKMS, CB, SQS, DSP, PBW, BAH. Jointly developed the structure and arguments for the paper: LKMS, CB, BAH. Made critical revisions and approved final version: SQS, DSP, PBW. All authors reviewed and approved of the final manuscript.

Disclosures and Ethics

As a requirement of publication author(s) have provided to the publisher signed confirmation of compliance with legal and ethical obligations including but not limited to the following: authorship and contributorship, conflicts of interest, privacy and confidentiality and (where applicable) protection of human and animal research subjects. The authors have read and confirmed their agreement with the ICMJE authorship and conflict of interest criteria. The authors have also confirmed that this article is unique and not under consideration or published in any other publication, and that they have permission from rights holders to reproduce any copyrighted material. Any disclosures are made in this section. The external blind peer reviewers report no conflicts of interest.

REFERENCES

1. Hunter EB, Johnston PE, Tanner G, Pinson CW, Awad JA. Bromfenac (Duract)-associated hepatic failure requiring liver transplantation. *Am J Gastroenterol*. 1999;94(8):2299–2301. doi:10.1111/j.1572-0241.1999.01321.x.
2. Kohlroser J, Mathai J, Reichheld J, Banner BF, Bonkovsky HL. Hepatotoxicity due to troglitazone: report of two cases and review of adverse events reported to the United States Food and Drug Administration. *Am J Gastroenterol*. 2000;95(1):272–276. doi:10.1111/j.1572-0241.2000.01707.x.
3. Lasser KE, Allen PD, Woolhandler SJ, Himmelstein DU, Wolfe SM, Bor DH. Timing of new black box warnings and withdrawals for prescription medications. *JAMA*. 2002;287(17):2215–2220.
4. Guengerich FP. Mechanisms of drug toxicity and relevance to pharmaceutical development. *Drug Metab Pharmacokinet*. 2011;26(1):3–14.
5. Jaeschke H, Xie Y, McGill MR. Acetaminophen-induced Liver Injury: from Animal Models to Humans. *J Clin Transl Hepatol*. 2014;2(3):153–161. doi:10.14218/JCTH.2014.00014.
6. Morgan RE, Trauner M, van Staden CJ, et al. Interference with bile salt export pump function is a susceptibility factor for human liver injury in drug development. *Toxicol Sci Off J Soc Toxicol*. 2010;118(2):485–500. doi:10.1093/toxsci/kfq269.
7. Morgan RE, van Staden CJ, Chen Y, et al. A multifactorial approach to hepatobiliary transporter assessment enables improved therapeutic compound development. *Toxicol Sci Off J Soc Toxicol*. 2013;136(1):216–241. doi:10.1093/toxsci/kft176.
8. Aleo M, Luo Y, Swiss R, Bonin P. Human drug-induced liver injury severity is highly associated to dual inhibition of liver mitochondrial function and bile salt export pump. *Hepatology*. 2014:1–33.
9. Chen M, Suzuki A, Borlak J, Andrade RJ, Isabel Lucena M. Drug-Induced liver injury: interactions between drug properties and host factors. *J Hepatol*. 2015;63(2):503–514. doi:10.1016/j.jhep.2015.04.016.
10. Paul WE. Bridging innate and adaptive immunity. *Cell*. 2011;147(6):1212–1215. doi:10.1016/j.cell.2011.11.036.
11. Palucka K, Banchereau J. Dendritic cells: a link between innate and adaptive immunity. *J Clin Immunol*. 1999;19(1):12–25.
12. Liu Z-X, Kaplowitz N. Role of innate immunity in acetaminophen-induced hepatotoxicity. *Expert Opin Drug Metab Toxicol*. 2006;2(4):493–503. doi:10.1517/17425255.2.4.493.
13. Jaeschke H, Williams CD, Ramachandran A, Bajt ML. Acetaminophen hepatotoxicity and repair: the role of sterile inflammation and innate immunity. *Liver Int Off J Int Assoc Study Liver*. 2012;32(1):8–20. doi:10.1111/j.1478-3231.2011.02501.x.
14. Kim SH, Naisbitt DJ. Update on Advances in Research on Idiosyncratic Drug-Induced Liver Injury. *Allergy Asthma Immunol Res*. 2016;8(1):3–11. doi:10.4168/aair.2016.8.1.3.
15. Yang K, Woodhead JL, Watkins PB, Howell BA, Brouwer KL. Systems Pharmacology Modeling Predicts Delayed Presentation and Species

Differences in Bile Acid-Mediated Troglitazone Hepatotoxicity. *Clin Pharmacol Ther*. July 2014:589–598. doi:10.1038/clpt.2014.158.
16. Shoda LKM, Woodhead JL, Siler SQ, Watkins PB, Howell BA. Linking physiology to toxicity using DILIsym(®), a mechanistic mathematical model of drug-induced liver injury. *Biopharm Drug Dispos*. 2014;35(1):33–49. doi:10.1002/bdd.1878.
17. Howell BA, Siler SQ, Watkins PB. Use of a systems model of drug-induced liver injury (DILIsym(®)) to elucidate the mechanistic differences between acetaminophen and its less-toxic isomer, AMAP, in mice. *Toxicol Lett*. 2014;226(2):163–172. doi:10.1016/j.toxlet.2014.02.007.
18. Longo DM, Yang Y, Watkins PB, Howell BA, Siler SQ. Elucidating Differences in the Hepatotoxic Potential of Tolcapone and Entacapone With DILIsym(®), a Mechanistic Model of Drug-Induced Liver Injury. *CPT Pharmacomet Syst Pharmacol*. 2016;5(1):31–39. doi:10.1002/psp4.12053.
19. Kurth MJ, Yokoi T, Gershwin ME. Halothane-induced hepatitis: paradigm or paradox for drug-induced liver injury. *Hepatol Baltim Md*. 2014;60(5):1473–1475. doi:10.1002/hep.27253.
20. Metushi IG, Hayes MA, Uetrecht J. Treatment of PD-1(-/-) mice with amodiaquine and anti-CTLA4 leads to liver injury similar to idiosyncratic liver injury in patients. *Hepatol Baltim Md*. 2015;61(4):1332–1342. doi:10.1002/hep.27549.
21. Metushi IG, Uetrecht J, Phillips E. Mechanism of isoniazid-induced hepatotoxicity: then and now. *Br J Clin Pharmacol*. January 2016. doi:10.1111/bcp.12885.
22. Hinson JA, Roberts DW, James LP. Mechanisms of acetaminophen-induced liver necrosis. *Handb Exp Pharmacol*. 2010;(196):369–405. doi:10.1007/978-3-642-00663-0_12.
23. Matzinger P. The danger model: a renewed sense of self. *Science*. 2002;296(5566):301–305. doi:10.1126/science.1071059.
24. Antoine DJ, Harris HE, Andersson U, Tracey KJ, Bianchi ME. A systematic nomenclature for the redox states of high mobility group box (HMGB) proteins. *Mol Med Camb Mass*. 2014;20:135–137. doi:10.2119/molmed.2014.00022.
25. Antoine DJ, Williams DP, Kipar A, et al. High-mobility group box-1 protein and keratin-18, circulating serum proteins informative of acetaminophen-induced necrosis and apoptosis in vivo. *Toxicol Sci Off J Soc Toxicol*. 2009;112(2):521–531. doi:10.1093/toxsci/kfp235.
26. Antoine DJ, Jenkins RE, Dear JW, et al. Molecular forms of HMGB1 and keratin-18 as mechanistic biomarkers for mode of cell death and prognosis during clinical acetaminophen hepatotoxicity. *J Hepatol*. 2012;56(5):1070–1079. doi:10.1016/j.jhep.2011.12.019.
27. Chen G-Y, Tang J, Zheng P, Liu Y. CD24 and Siglec-10 selectively repress tissue damage-induced immune responses. *Science*. 2009;323(5922):1722–1725. doi:10.1126/science.1168988.
28. Antoine DJ, Williams DP, Kipar A, Laverty H, Park BK. Diet restriction inhibits apoptosis and HMGB1 oxidation and promotes inflammatory cell recruitment during acetaminophen hepatotoxicity. *Mol Med Camb Mass*. 2010;16(11-12):479–490. doi:10.2119/molmed.2010.00126.
29. Yang R, Zhang S, Cotoia A, Oksala N, Zhu S, Tenhunen J. High mobility group B1 impairs hepatocyte regeneration in acetaminophen hepatotoxicity. *BMC Gastroenterol*. 2012;12(1):45. doi:10.1186/1471-230X-12-45.
30. Huebener P, Pradere J-P, Hernandez C, et al. The HMGB1/RAGE axis triggers neutrophil-mediated injury amplification following necrosis. *J Clin Invest*. 2015;125(2):539–550. doi:10.1172/JCI76887.
31. Scaffidi P, Misteli T, Bianchi ME. Release of chromatin protein HMGB1 by necrotic cells triggers inflammation. *Nature*. 2002;418(6894):191–195. doi:10.1038/nature00858.
32. Park JS, Svetkauskaite D, He Q, et al. Involvement of toll-like receptors 2 and 4 in cellular activation by high mobility group box 1 protein. *J Biol Chem*. 2004;279(9):7370–7377. doi:10.1074/jbc.M306793200.
33. Sha Y, Zmijewski J, Xu Z, Abraham E. HMGB1 develops enhanced proinflammatory activity by binding to cytokines. *J Immunol Baltim Md 1950*. 2008;180(4):2531–2537.
34. Horst AK, Neumann K, Diehl L, Tiegs G. Modulation of liver tolerance by conventional and nonconventional antigen-presenting cells and regulatory immune cells. *Cell Mol Immunol*. 2016;13(3):277–292. doi:10.1038/cmi.2015.112.
35. Heymann F, Peusquens J, Ludwig-Portugall I, et al. Liver inflammation abrogates immunological tolerance induced by Kupffer cells. *Hepatol Baltim Md*. 2015;62(1):279-291. doi:10.1002/hep.27793.
36. You Q, Cheng L, Kedl RM, Ju C. Mechanism of T cell tolerance induction by murine hepatic Kupffer cells. *Hepatol Baltim Md*. 2008;48(3):978–990. doi:10.1002/hep.22395.
37. Kato T, Ito Y, Hosono K, et al. Vascular endothelial growth factor receptor-1 signaling promotes liver repair through restoration of liver microvasculature after acetaminophen hepatotoxicity. *Toxicol Sci Off J Soc Toxicol*. 2011;120(1):218–229. doi:10.1093/toxsci/kfq366.
38. Luedde T, Kaplowitz N, Schwabe RF. Cell Death and Cell Death Responses in Liver Disease: Mechanisms and Clinical Relevance. *Gastroenterology*. July 2014. doi:10.1053/j.gastro.2014.07.018.
39. Schwabe RF, Brenner DA. Mechanisms of Liver Injury. I. TNF-alpha-induced liver injury: role of IKK, JNK, and ROS pathways. *Am J Physiol Gastrointest Liver Physiol*. 2006;290(4):G583–589. doi:10.1152/ajpgi.00422.2005.
40. Liu Z-X, Govindarajan S, Kaplowitz N. Innate immune system plays a critical role in determining the progression and severity of acetaminophen hepatotoxicity. *Gastroenterology*. 2004;127(6):1760–1774.
41. Liu Z-X, Han D, Gunawan B, Kaplowitz N. Neutrophil depletion protects against murine acetaminophen hepatotoxicity. *Hepatol Baltim Md*. 2006;43(6):1220–1230. doi:10.1002/hep.21175.
42. Ishida Y, Kondo T, Kimura A, Tsuneyama K, Takayasu T, Mukaida N. Opposite roles of neutrophils and macrophages in the pathogenesis of acetaminophen-induced acute liver injury. *Eur J Immunol*. 2006;36(4):1028–1038. doi:10.1002/eji.200535261.
43. Jaeschke H. Innate immunity and acetaminophen-induced liver injury: why so many controversies? *Hepatol Baltim Md*. 2008;48(3):699–701. doi:10.1002/hep.22556.
44. Ju C, Reilly TP, Bourdi M, et al. Protective role of Kupffer cells in acetaminophen-induced hepatic injury in mice. *Chem Res Toxicol*. 2002;15(12):1504-1513.
45. Campion SN, Johnson R, Aleksunes LM, et al. Hepatic Mrp4 induction following acetaminophen exposure is dependent on Kupffer cell function. *Am J Physiol Gastrointest Liver Physiol*. 2008;295(2):G294–304. doi:10.1152/ajpgi.00541.2007.
46. Fisher JE, McKenzie TJ, Lillegard JB, et al. Role of Kupffer cells and toll-like receptor 4 in acetaminophen-induced acute liver failure. *J Surg Res*. 2013;180(1):147–155. doi:10.1016/j.jss.2012.11.051.
47. You Q, Holt M, Yin H, Li G, Hu C-J, Ju C. Role of hepatic resident and infiltrating macrophages in liver repair after acute injury. *Biochem Pharmacol*. 2013;86(6):836–843. doi:10.1016/j.bcp.2013.07.006.
48. Marques PE, Oliveira AG, Pereira RV, et al. Hepatic DNA deposition drives drug-induced liver injury and inflammation in mice. *Hepatol Baltim Md*. 2015;61(1):348–360. doi:10.1002/hep.27216.
49. DeLeve LD, Wang X, Kaplowitz N, Shulman HM, Bart JA, van der Hoek A. Sinusoidal endothelial cells as a target for acetaminophen toxicity. Direct action versus requirement for hepatocyte activation in different mouse strains. *Biochem Pharmacol*. 1997;53(9):1339–1345.
50. Ito Y, Bethea NW, Abril ER, McCuskey RS. Early hepatic microvascular injury in response to acetaminophen toxicity. *Microcirc N Y N 1994*. 2003;10(5):391–400. doi:10.1038/sj.mn.7800204.
51. Holt MP, Yin H, Ju C. Exacerbation of acetaminophen-induced disturbances of liver sinusoidal endothelial cells in the absence of Kupffer cells in mice. *Toxicol Lett*. 2010;194(1-2):34–41. doi:10.1016/j.toxlet.2010.01.020.
52. Wu W-K, Llewellyn OPC, Bates DO, Nicholson LB, Dick AD. IL-10 regulation of macrophage VEGF production is dependent on macrophage polarisation and hypoxia. *Immunobiology*. 2010;215(9-10):796–803. doi:10.1016/j.imbio.2010.05.025.
53. Fiuza C, Bustin M, Talwar S, et al. Inflammation-promoting activity of HMGB1 on human microvascular endothelial cells. *Blood*. 2003;101(7):2652–2660. doi:10.1182/blood-2002-05-1300.
54. Andersson U, Wang H, Palmblad K, et al. High mobility group 1 protein (HMG-1) stimulates proinflammatory cytokine synthesis in human monocytes. *J Exp Med*. 2000;192(4):565–570.
55. Yang H, Antoine DJ, Andersson U, Tracey KJ. The many faces of HMGB1: molecular structure-functional activity in inflammation, apoptosis, and chemotaxis. *J Leukoc Biol*. 2013;93(6):865–873. doi:10.1189/jlb.1212662.
56. LeCouter J, Moritz DR, Li B, et al. Angiogenesis-independent endothelial protection of liver: role of VEGFR-1. *Science*. 2003;299(5608):890–893. doi:10.1126/science.1079562.
57. Knolle PA, Löser E, Protzer U, et al. Regulation of endotoxin-induced IL-6 production in liver sinusoidal endothelial cells and Kupffer cells by IL-10. *Clin Exp Immunol*. 1997;107(3):555–561.
58. Fiorentino DF, Zlotnik A, Mosmann TR, Howard M, O'Garra A. IL-10 inhibits cytokine production by activated macrophages. *J Immunol Baltim Md 1950*. 1991;147(11):3815–3822.
59. Yang H, Hreggvidsdottir HS, Palmblad K, et al. A critical cysteine is required for HMGB1 binding to Toll-like receptor 4 and activation of macrophage cytokine release. *Proc Natl Acad Sci U S A*. 2010;107(26):11942–11947. doi:10.1073/pnas.1003893107.
60. Schiraldi M, Raucci A, Muñoz LM, et al. HMGB1 promotes recruitment of inflammatory cells to damaged tissues by forming a complex with CXCL12 and signaling via CXCR4. *J Exp Med*. 2012;209(3):551–563. doi:10.1084/jem.20111739.
61. Essani NA, Bajt ML, Farhood A, Vonderfecht SL, Jaeschke H. Transcriptional activation of vascular cell adhesion molecule-1 gene in vivo and its role in the pathophysiology of neutrophil-induced liver injury in murine endotoxin shock. *J Immunol Baltim Md 1950*. 1997;158(12):5941–5948.
62. Shnyra A, Brewington R, Alipio A, Amura C, Morrison DC. Reprogramming of lipopolysaccharide-primed macrophages is controlled by a counterbalanced

production of IL-10 and IL-12. *J Immunol Baltim Md 1950*. 1998;160(8): 3729–3736.
63. Bonaldi T, Talamo F, Scaffidi P, et al. Monocytic cells hyperacetylate chromatin protein HMGB1 to redirect it towards secretion. *EMBO J*. 2003;22(20):5551–5560. doi:10.1093/emboj/cdg516.
64. Chen G, Li J, Ochani M, et al. Bacterial endotoxin stimulates macrophages to release HMGB1 partly through CD14- and TNF-dependent mechanisms. *J Leukoc Biol*. 2004;76(5):994–1001. doi:10.1189/jlb.0404242.
65. Smith D, Lackides G, Epstein L. Coordinated induction of autocrine tumor necrosis factor and interleukin 1 in normal human monocytes and the implications for monocyte-mediated cytotoxicity. *Cancer Res*. 1990;50:3146–3153.
66. Ding B-S, Nolan DJ, Butler JM, et al. Inductive angiocrine signals from sinusoidal endothelium are required for liver regeneration. *Nature*. 2010;468(7321):310–315. doi:10.1038/nature09493.
67. Leibovich SJ, Chen J-F, Pinhal-Enfield G, et al. Synergistic up-regulation of vascular endothelial growth factor expression in murine macrophages by adenosine A(2A) receptor agonists and endotoxin. *Am J Pathol*. 2002;160(6):2231–2244. doi:10.1016/S0002-9440(10)61170-4.
68. Webber EM, Bruix J, Pierce RH, Fausto N. Tumor necrosis factor primes hepatocytes for DNA replication in the rat. *Hepatol Baltim Md*. 1998;28(5):1226–1234. doi:10.1002/hep.510280509.
69. Cosgrove BD, Cheng C, Pritchard JR, Stolz DB, Lauffenburger DA, Griffith LG. An inducible autocrine cascade regulates rat hepatocyte proliferation and apoptosis responses to tumor necrosis factor-alpha. *Hepatol Baltim Md*. 2008;48(1):276–288. doi:10.1002/hep.22335.
70. Gallucci RM, Simeonova PP, Toriumi W, Luster MI. TNF-alpha Regulates Transforming Growth Factor- Expression in Regenerating Murine Liver and Isolated Hepatocytes. *J Immunol*. 2000;164(2):872–878. doi:10.4049/jimmunol.164.2.872.
71. Kazama H, Ricci J-E, Herndon JM, Hoppe G, Green DR, Ferguson TA. Induction of immunological tolerance by apoptotic cells requires caspase-dependent oxidation of high-mobility group box-1 protein. *Immunity*. 2008;29(1):21–32. doi:10.1016/j.immuni.2008.05.013.
72. Bianchi ME. HMGB1 loves company. *J Leukoc Biol*. 2009;86(3):573–576. doi:10.1189/jlb.1008585.
73. Leist M, Single B, Castoldi AF, Kühnle S, Nicotera P. Intracellular adenosine triphosphate (ATP) concentration: a switch in the decision between apoptosis and necrosis. *J Exp Med*. 1997;185(8):1481–1486.
74. de Waal Malefyt R, Abrams J, Bennett B, Figdor CG, de Vries JE. Interleukin 10(IL-10) inhibits cytokine synthesis by human monocytes: an autoregulatory role of IL-10 produced by monocytes. *J Exp Med*. 1991;174(5):1209–1220.
75. Yee SB, Bourdi M, Masson MJ, Pohl LR. Hepatoprotective role of endogenous interleukin-13 in a murine model of acetaminophen-induced liver disease. *Chem Res Toxicol*. 2007;20(5):734–744. doi:10.1021/tx600349f.
76. Williams CD, Farhood A, Jaeschke H. Role of caspase-1 and interleukin-1beta in acetaminophen-induced hepatic inflammation and liver injury. *Toxicol Appl Pharmacol*. 2010;247(3):169–178. doi:10.1016/j.taap.2010.07.004.
77. Merrick BA, Bruno ME, Madenspacher JH, et al. Alterations in the rat serum proteome during liver injury from acetaminophen exposure. *J Pharmacol Exp Ther*. 2006;318(2):792–802. doi:10.1124/jpet.106.102681.
78. Arafa HMM. Carnitine deficiency: a possible risk factor in paracetamol hepatotoxicity. *Arch Toxicol*. 2009;83(2):139-150. doi:10.1007/s00204-008-0330-x.
79. Antoniades CG, Berry PA, Davies ET, et al. Reduced monocyte HLA-DR expression: a novel biomarker of disease severity and outcome in acetaminophen-induced acute liver failure. *Hepatol Baltim Md*. 2006;44(1):34–43. doi:10.1002/hep.21240.
80. Antoniades CG, Quaglia A, Taams LS, et al. Source and characterisation of hepatic macrophages in acetaminophen-induced acute liver failure in humans. *Hepatol Baltim Md*. February 2012. doi:10.1002/hep.25657.
81. Berry PA, Antoniades CG, Hussain MJ, et al. Admission levels and early changes in serum interleukin-10 are predictive of poor outcome in acute liver failure and decompensated cirrhosis. *Liver Int Off J Int Assoc Study Liver*. 2010;30(5):733–740. doi:10.1111/j.1478-3231.2010.02219.x.
82. Mookerjee RP, Dalton RN, Davies NA, et al. Inflammation is an important determinant of levels of the endogenous nitric oxide synthase inhibitor asymmetric dimethylarginine (ADMA) in acute liver failure. *Liver Transplant Off Publ Am Assoc Study Liver Dis Int Liver Transplant Soc*. 2007;13(3):400–405. doi:10.1002/lt.21053.
83. Rutherford AE, Hynan LS, Borges CBS, et al. Serum apoptosis markers in acute liver failure: a pilot study. *Clin Gastroenterol Hepatol Off Clin Pract J Am Gastroenterol Assoc*. 2007;5(12):1477–1483. doi:10.1016/j.cgh.2007.08.007.
84. Blazka ME, Elwell MR, Holladay SD, Wilson RE, Luster MI. Histopathology of acetaminophen-induced liver changes: role of interleukin 1 alpha and tumor necrosis factor alpha. *Toxicol Pathol*. 1996;24(2):181–189.
85. Blazka ME, Wilmer JL, Holladay SD, Wilson RE, Luster MI. Role of proinflammatory cytokines in acetaminophen hepatotoxicity. *Toxicol Appl Pharmacol*. 1995;133(1):43–52. doi:10.1006/taap.1995.1125.
86. Ishida Y, Kondo T, Tsuneyama K, Lu P, Takayasu T, Mukaida N. The pathogenic roles of tumor necrosis factor receptor p55 in acetaminophen-induced liver injury in mice. *J Leukoc Biol*. 2004;75(1):59–67. doi:10.1189/jlb.0403152.
87. Simpson KJ, Lukacs NW, McGregor AH, Harrison DJ, Strieter RM, Kunkel SL. Inhibition of tumour necrosis factor alpha does not prevent experimental paracetamol-induced hepatic necrosis. *J Pathol*. 2000;190(4):489–494. doi:10.1002/(SICI)1096-9896(200003)190:4<489::AID-PATH534>3.0.CO;2-V.
88. Chiu H, Gardner CR, Dambach DM, et al. Role of tumor necrosis factor receptor 1 (p55) in hepatocyte proliferation during acetaminophen-induced toxicity in mice. *Toxicol Appl Pharmacol*. 2003;193(2):218–227.
89. Boess F, Bopst M, Althaus R, et al. Acetaminophen hepatotoxicity in tumor necrosis factor/lymphotoxin-alpha gene knockout mice. *Hepatol Baltim Md*. 1998;27(4):1021–1029. doi:10.1002/hep.510270418.
90. Frith JC, Mönkkönen J, Auriola S, Mönkkönen H, Rogers MJ. The molecular mechanism of action of the antiresorptive and antiinflammatory drug clodronate: evidence for the formation in vivo of a metabolite that inhibits bone resorption and causes osteoclast and macrophage apoptosis. *Arthritis Rheum*. 2001;44(9):2201–2210.
91. Nikolic T, Geutskens SB, van Rooijen N, Drexhage HA, Leenen PJM. Dendritic cells and macrophages are essential for the retention of lymphocytes in (peri)-insulitis of the nonobese diabetic mouse: a phagocyte depletion study. *Lab Investig J Tech Methods Pathol*. 2005;85(4):487–501. doi:10.1038/labinvest.3700238.
92. Yamamoto T, Naito M, Moriyama H, et al. Repopulation of murine Kupffer cells after intravenous administration of liposome-encapsulated dichloromethylene diphosphonate. *Am J Pathol*. 1996;149(4):1271–1286.
93. Van Rooijen N, Kors N, vd Ende M, Dijkstra CD. Depletion and repopulation of macrophages in spleen and liver of rat after intravenous treatment with liposome-encapsulated dichloromethylene diphosphonate. *Cell Tissue Res*. 1990;260(2):215–222.
94. Radi ZA, Koza-Taylor PH, Bell RR, et al. Increased serum enzyme levels associated with kupffer cell reduction with no signs of hepatic or skeletal muscle injury. *Am J Pathol*. 2011;179(1):240–247. doi:10.1016/j.ajpath.2011.03.029.
95. Cover C, Liu J, Farhood A, et al. Pathophysiological role of the acute inflammatory response during acetaminophen hepatotoxicity. *Toxicol Appl Pharmacol*. 2006;216(1):98-107. doi:10.1016/j.taap.2006.04.010.
96. Jaeschke H, Williams CD, McGill MR, Xie Y, Ramachandran A. Models of drug-induced liver injury for evaluation of phytotherapeutics and other natural products. *Food Chem Toxicol Int J Publ Br Ind Biol Res Assoc*. 2013;55:279–289. doi:10.1016/j.fct.2012.12.063.
97. Knockaert L, Berson A, Ribault C, et al. Carbon tetrachloride-mediated lipid peroxidation induces early mitochondrial alterations in mouse liver. *Lab Investig J Tech Methods Pathol*. 2012;92(3):396–410. doi:10.1038/labinvest.2011.193.
98. Albano E, Bellomo G, Carini R, Biasi F, Poli G, Dianzani MU. Mechanisms responsible for carbon tetrachloride-induced perturbation of mitochondrial calcium homeostasis. *FEBS Lett*. 1985;192(2):184–188.
99. van Furth R, Sluiter W. Distribution of blood monocytes between a marginating and a circulating pool. *J Exp Med*. 1986;163(2):474–479.
100. Crofton RW, Diesselhoff-den Dulk MM, van Furth R. The origin, kinetics, and characteristics of the Kupffer cells in the normal steady state. *J Exp Med*. 1978;148(1):1–17.
101. Chanda S, Mehendale HM. Hepatic cell division and tissue repair: a key to survival after liver injury. *Mol Med Today*. 1996;2(2):82–89.
102. van Furth R, Elzenga-Claasen I, van Schadewijk-Nieuwstad M, Diesselhoff-den Dulk MM, Toivonen H, Rytömaa T. Cell kinetic analysis of a murine macrophage cell line. *Eur J Cell Biol*. 1987;44(1):93–96.
103. Guilbert LJ, Winkler-Lowen B, Smith A, Branch DR, Garcia-Lloret M. Analysis of the synergistic stimulation of mouse macrophage proliferation by macrophage colony-stimulating factor (CSF-1) and tumor necrosis factor alpha (TNF-alpha). *J Leukoc Biol*. 1993;54(1):65–72.
104. Sawyer RT. The significance of local resident pulmonary alveolar macrophage proliferation to population renewal. *J Leukoc Biol*. 1986;39(1):77–87.
105. Brown RP, Delp MD, Lindstedt SL, Rhomberg LR, Beliles RP. Physiological parameter values for physiologically based pharmacokinetic models. *Toxicol Ind Health*. 1997;13(4):407–484.
106. Sleyster EC, Knook DL. Relation between localization and function of rat liver Kupffer cells. *Lab Investig J Tech Methods Pathol*. 1982;47(5):484–490.
107. Wisse E, Braet F, Luo D, et al. Structure and function of sinusoidal lining cells in the liver. *Toxicol Pathol*. 1996;24(1):100–111.
108. Bouwens L, Knook DL, Wisse E. Local proliferation and extrahepatic recruitment of liver macrophages (Kupffer cells) in partial-body irradiated rats. *J Leukoc Biol*. 1986;39(6):687–697.
109. EDWARDS JL, KLEIN RE. Cell renewal in adult mouse tissues. *Am J Pathol*. 1961;38:437–453.

110. KELLY LS, BROWN BA, DOBSON EL. Cell division and phagocytic activity in liver reticulo-endothelial cells. *Proc Soc Exp Biol Med Soc Exp Biol Med N Y N*. 1962;110:555–559.
111. Mathew J, Hines JE, James OF, Burt AD. Non-parenchymal cell responses in paracetamol (acetaminophen)-induced liver injury. *J Hepatol*. 1994;20(4):537–541.
112. North RJ. The mitotic potential of fixed phagocytes in the liver as revealed during the development of cellular immunity. *J Exp Med*. 1969;130(2): 315–326.
113. Volkman A. Disparity in origin of mononuclear phagocyte populations. *J Reticuloendothel Soc*. 1976;19(4):249–268.
114. Hobson B, Denekamp J. Endothelial proliferation in tumours and normal tissues: continuous labelling studies. *Br J Cancer*. 1984;49(4):405–413.
115. Tannock IF, Hayashi S. The proliferation of capillary endothelial cells. *Cancer Res*. 1972;32(1):77–82.
116. Ohnishi T, Arnold LL, Clark NM, Wisecarver JL, Cohen SM. Comparison of endothelial cell proliferation in normal liver and adipose tissue in B6C3F1 mice, F344 rats, and humans. *Toxicol Pathol*. 2007;35(7):904–909. doi:10.1080/01926230701748081.
117. Rubin DB, Drab EA, Ward WF, Bauer KD. Cell cycle progression in irradiated endothelial cells cultured from bovine aorta. *Radiat Res*. 1988;116(2):364–371.
118. Bourdi M, Eiras DP, Holt MP, et al. Role of IL-6 in an IL-10 and IL-4 double knockout mouse model uniquely susceptible to acetaminophen-induced liver injury. *Chem Res Toxicol*. 2007;20(2):208–216. doi:10.1021/tx060228l.
119. Wu Y-L, Piao D-M, Han X-H, Nan J-X. Protective effects of salidroside against acetaminophen-induced toxicity in mice. *Biol Pharm Bull*. 2008;31(8):1523–1529.
120. Yuan H-D, Jin G-Z, Piao G-C. Hepatoprotective effects of an active part from Artemisia sacrorum Ledeb. against acetaminophen-induced toxicity in mice. *J Ethnopharmacol*. 2010;127(2):528–533. doi:10.1016/j.jep.2009.10.002.
121. Martin-Murphy BV, Holt MP, Ju C. The role of damage associated molecular pattern molecules in acetaminophen-induced liver injury in mice. *Toxicol Lett*. 2010;192(3):387–394. doi:10.1016/j.toxlet.2009.11.016.
122. Hasegawa A, Iwasaka H, Hagiwara S, Asai N, Nishida T, Noguchi T. Alternate day calorie restriction improves systemic inflammation in a mouse model of sepsis induced by cecal ligation and puncture. *J Surg Res*. 2012;174(1):136–141. doi:10.1016/j.jss.2010.11.883.
123. Watanabe T, Kubota S, Nagaya M, et al. The role of HMGB-1 on the development of necrosis during hepatic ischemia and hepatic ischemia/reperfusion injury in mice. *J Surg Res*. 2005;124(1):59–66. doi:10.1016/j.jss.2004.10.019.
124. Gohda E, Yamasaki T, Tsubouchi H, et al. Biological and immunological properties of human hepatocyte growth factor from plasma of patients with fulminant hepatic failure. *Biochim Biophys Acta*. 1990;1053(1):21–26.
125. Sgroi A, Mai G, Morel P, et al. Transplantation of encapsulated hepatocytes during acute liver failure improves survival without stimulating native liver regeneration. *Cell Transplant*. 2011;20(11-12):1791–1803. doi:10.3727/096368911X564976.
126. GRISHAM JW. A morphologic study of deoxyribonucleic acid synthesis and cell proliferation in regenerating rat liver; autoradiography with thymidine-H3. *Cancer Res*. 1962;22:842–849.
127. Ding JW, Wang K, Brems JJ, Gamelli RL. Protection against concanavalin A-induced hepatocyte apoptosis by molsidomine is time-dependent. *J Am Coll Surg*. 2004;198(1):67–77. doi:10.1016/j.jamcollsurg.2003.08.014.
128. Bursch W, Paffe S, Putz B, Barthel G, Schulte-Hermann R. Determination of the length of the histological stages of apoptosis in normal liver and in altered hepatic foci of rats. *Carcinogenesis*. 1990;11(5):847–853.
129. Oberhammer F, Nagy P, Tiefenbacher R, et al. The antiandrogen cyproterone acetate induces synthesis of transforming growth factor beta 1 in the parenchymal cells of the liver accompanied by an enhanced sensitivity to undergo apoptosis and necrosis without inflammation. *Hepatol Baltim Md*. 1996;23(2):329–337. doi:10.1002/hep.510230220.
130. Wang H, Bloom O, Zhang M, et al. HMG-1 as a late mediator of endotoxin lethality in mice. *Science*. 1999;285(5425):248–251.
131. Müller S, Ronfani L, Bianchi ME. Regulated expression and subcellular localization of HMGB1, a chromatin protein with a cytokine function. *J Intern Med*. 2004;255(3):332–343.
132. Whitelaw DM. The intravascular lifespan of monocytes. *Blood*. 1966;28(3):455–464.
133. DeCicco LA, Rikans LE, Tutor CG, Hornbrook KR. Serum and liver concentrations of tumor necrosis factor alpha and interleukin-1beta following administration of carbon tetrachloride to male rats. *Toxicol Lett*. 1998;98(1-2):115–121.
134. Nakamoto N, Tada S, Kameyama K, et al. A free radical scavenger, edaravone, attenuates steatosis and cell death via reducing inflammatory cytokine production in rat acute liver injury. *Free Radic Res*. 2003;37(8):849–859.
135. Hagiwara S, Iwasaka H, Hidaka S, Hishiyama S, Noguchi T. Danaparoid sodium inhibits systemic inflammation and prevents endotoxin-induced acute lung injury in rats. *Crit Care Lond Engl*. 2008;12(2):R43. doi:10.1186/cc6851.
136. Hagiwara S, Iwasaka H, Hasegawa A, Asai N, Noguchi T. High-dose intravenous immunoglobulin G improves systemic inflammation in a rat model of CLP-induced sepsis. *Intensive Care Med*. 2008;34(10):1812–1819. doi:10.1007/s00134-008-1161-1.
137. Koga H, Hagiwara S, Inomata M, et al. The new vitamin E derivative, ETS-GS, protects against cecal ligation and puncture-induced systemic inflammation in rats. *Inflammation*. 2012;35(2):545–553. doi:10.1007/s10753-011-9344-2.
138. Liu A, Dirsch O, Fang H, et al. HMGB1 translocation and expression is caused by warm ischemia reperfusion injury, but not by partial hepatectomy in rats. *Exp Mol Pathol*. 2011;91(2):502–508. doi:10.1016/j.yexmp.2011.05.005.
139. Liu A, Dirsch O, Fang H, et al. HMGB1 in ischemic and non-ischemic liver after selective warm ischemia/reperfusion in rat. *Histochem Cell Biol*. 2011;135(5):443–452. doi:10.1007/s00418-011-0802-6.
140. Koga H, Hagiwara S, Inomata M, et al. Vitamin E derivative ETS-GS reduces liver ischemia-reperfusion injury in rats. *J Surg Res*. 2012;175(1):118–122. doi:10.1016/j.jss.2011.02.045.
141. Oishi K, Hagiwara S, Koga S, et al. The Vitamin E Derivative, EPC-K1, Suppresses Inflammation During Hepatic Ischemia-Reperfusion Injury and Exerts Hepatoprotective Effects in Rats. *J Surg Res*. 2012;176(1):164–170. doi:10.1016/j.jss.2011.03.080.
142. Swain MG, Appleyard C, Wallace J, Wong H, Le T. Endogenous glucocorticoids released during acute toxic liver injury enhance hepatic IL-10 synthesis and release. *Am J Physiol*. 1999;276(1 Pt 1):G199–205.
143. Lindroos PM, Zarnegar R, Michalopoulos GK. Hepatocyte growth factor (hepatopoietin A) rapidly increases in plasma before DNA synthesis and liver regeneration stimulated by partial hepatectomy and carbon tetrachloride administration. *Hepatol Baltim Md*. 1991;13(4):743–750.
144. Zhu C, Li Y, Li W, Wu Q, Gao R. Gene transfer of c-met confers protection against D-galactosamine/lipopolysaccharide-induced acute liver failure. Dig Dis Sci. 2012;57(4):925–934. doi:10.1007/s10620-012-2052-4.
145. Kinoshita T, Hirao S, Matsumoto K, Nakamura T. Possible endocrine control by hepatocyte growth factor of liver regeneration after partial hepatectomy. *Biochem Biophys Res Commun*. 1991;177(1):330–335.
146. Whitelaw DM. Observations on human monocyte kinetics after pulse labeling. *Cell Tissue Kinet*. 1972;5(4):311–317.
147. Oshima G, Shinoda M, Tanabe M, et al. Increased plasma levels of high mobility group box 1 in patients with acute liver failure. *Eur Surg Res Eur Chir Forsch Rech Chir Eur*. 2012;48(3):154–162. doi:10.1159/000338363.
148. Ilmakunnas M, Tukiainen EM, Rouhiainen A, et al. High mobility group box 1 protein as a marker of hepatocellular injury in human liver transplantation. *Liver Transplant Off Publ Am Assoc Study Liver Dis Int Liver Transplant Soc*. 2008;14(10):1517–1525. doi:10.1002/lt.21573.
149. Ueno H, Matsuda T, Hashimoto S, et al. Contributions of high mobility group box protein in experimental and clinical acute lung injury. *Am J Respir Crit Care Med*. 2004;170(12):1310-1316. doi:10.1164/rccm.200402-188OC.
150. Miwa Y, Harrison PM, Farzaneh F, Langley PG, Williams R, Hughes RD. Plasma levels and hepatic mRNA expression of transforming growth factor-beta1 in patients with fulminant hepatic failure. *J Hepatol*. 1997;27(5): 780–788.
151. Hughes RD, Zhang L, Tsubouchi H, Daikuhara Y, Williams R. Plasma hepatocyte growth factor and biliprotein levels and outcome in fulminant hepatic failure. *J Hepatol*. 1994;20(1):106–111.
152. Efimova EA, Glanemann M, Nussler AK, et al. Changes in serum levels of growth factors in healthy individuals after living related liver donation. *Transplant Proc*. 2005;37(2):1074–1075. doi:10.1016/j.transproceed.2004.12.170.
153. Lawson JA, Farhood A, Hopper RD, Bajt ML, Jaeschke H. The hepatic inflammatory response after acetaminophen overdose: role of neutrophils. *Toxicol Sci Off J Soc Toxicol*. 2000;54(2):509–516.
154. Saha B, Nandi D. Farnesyltransferase inhibitors reduce Ras activation and ameliorate acetaminophen-induced liver injury in mice. *Hepatol Baltim Md*. 2009;50(5):1547–1557. doi:10.1002/hep.23180.
155. Goldin RD, Ratnayaka ID, Breach CS, Brown IN, Wickramasinghe SN. Role of macrophages in acetaminophen (paracetamol)-induced hepatotoxicity. *J Pathol*. 1996;179(4):432–435. doi:10.1002/(SICI)1096-9896(199608)179:4<432::AID-PATH609>3.0.CO;2-S.
156. Jiang W, Gao M, Sun S, et al. Protective effect of L-theanine on carbon tetrachloride-induced acute liver injury in mice. *Biochem Biophys Res Commun*. 2012;422(2):344–350. doi:10.1016/j.bbrc.2012.05.022.
157. Ikejima K, Honda H, Yoshikawa M, et al. Leptin augments inflammatory and profibrogenic responses in the murine liver induced by hepatotoxic chemicals. *Hepatol Baltim Md*. 2001;34(2):288–297. doi:10.1053/jhep.2001.26518.
158. Louis H, Van Laethem JL, Wu W, et al. Interleukin-10 controls neutrophilic infiltration, hepatocyte proliferation, and liver fibrosis induced by carbon tetrachloride in mice. *Hepatol Baltim Md*. 1998;28(6):1607–1615. doi:10.1002/hep.510280621.

159. Morio LA, Chiu H, Sprowles KA, et al. Distinct roles of tumor necrosis factor-alpha and nitric oxide in acute liver injury induced by carbon tetrachloride in mice. *Toxicol Appl Pharmacol*. 2001;172(1):44–51. doi:10.1006/taap.2000.9133.
160. Lee C-P, Shih P-H, Hsu C-L, Yen G-C. Hepatoprotection of tea seed oil (Camellia oleifera Abel.) against CCl4-induced oxidative damage in rats. *Food Chem Toxicol Int J Publ Br Ind Biol Res Assoc*. 2007;45(6):888–895. doi:10.1016/j.fct.2006.11.007.
161. Bruccoleri A, Gallucci R, Germolec DR, et al. Induction of early-immediate genes by tumor necrosis factor alpha contribute to liver repair following chemical-induced hepatotoxicity. *Hepatol Baltim Md*. 1997;25(1):133–141. doi:10.1002/hep.510250125.
162. Shibata H, Yoshioka Y, Ohkawa A, et al. The therapeutic effect of TNFR1-selective antagonistic mutant TNF-alpha in murine hepatitis models. *Cytokine*. 2008;44(2):229–233. doi:10.1016/j.cyto.2008.07.003.